

**An intestinal organ culture system uncovers a role for the nervous  
system in microbe/immunocyte crosstalk**

*Nissan Yissachar<sup>1</sup>, Yan Zhou<sup>1</sup>, Lloyd Ung<sup>2,3</sup>, Nicole Y. Lai<sup>1</sup>, James F. Mohan<sup>1</sup>,  
Allen Ehrlicher<sup>2,3</sup>, David A. Weitz<sup>2,3</sup>, Dennis L. Kasper<sup>1</sup>, Isaac M. Chiu<sup>1\*</sup>, Diane Mathis<sup>1\*</sup>  
and Christophe Benoist<sup>1\*†</sup>*

<sup>1</sup>Division of Immunology, Department of Microbiology and Immunobiology, Harvard  
Medical School;

<sup>2</sup>School of Engineering and Applied Sciences, Harvard University

<sup>3</sup>Department of Physics, Harvard University

<sup>†</sup>Lead Author

\*Correspondence to:

Isaac Chiu, Diane Mathis and Christophe Benoist

Division of Immunology

Harvard Medical School

77 Avenue Louis Pasteur, Boston, MA 02115

e-mail: isaac\_chiu@hms.harvard.edu or cbdm@hms.harvard.edu

Phone: (617) 432-7741

## SUMMARY

Investigation of host-environment interactions in the gut would benefit from a culture system that maintained tissue architecture yet allowed tight experimental control. We devised a microfabricated organ culture system that viably preserves the normal multicellular composition of the mouse intestine, with luminal flow to control perturbations (e.g. microbes, drugs). It enables studying short-term responses of diverse gut components (immune, neuronal...). We focused on the early response to bacteria that induce either Th17 or RORg<sup>+</sup> T-regulatory (Treg) cells *in vivo*. Transcriptional responses partially reproduced *in vivo* signatures, but these microbes elicited diametrically opposite changes in expression of a neuronal-specific geneset, notably nociceptive neuropeptides. We demonstrated activation of sensory neurons by microbes, correlating with RORg<sup>+</sup> Treg induction. Colonic RORg<sup>+</sup> Treg frequencies increased in mice lacking TAC1 neuropeptide precursor, and decreased in capsaicin-diet fed mice. Thus, differential engagement of the enteric nervous system may partake in bifurcating pro- or anti-inflammatory responses to microbes.

A fundamental design principle of biological tissues is the tight relationship between tissue structure and function, where the differentiated cell-types that constitute the tissue are carefully arrayed to enable their functional interplay. In the intestines, the spatial organization of different cellular systems (epithelial, immune, neural), structural elements (mucus layer, tight junctions) and the luminal content (food, microbes), is particularly important. A careful balance must be struck between immune tolerance of necessary symbiotic microbes and the maintenance of a tight barrier to prevent tissue invasion by luminal microbes. In addition, regulatory systems must prevent potent microbial products from triggering inflammation and its collateral damage.

With the growing realization that symbiotic microbes help educate and tune the immune system (Hooper et al., 2012; Mowat and Agace, 2014), there is a need for experimental systems to finely analyze host-microbiota interactions. We know, just for the immune system, that the host/microbiome duet engages a bewildering array of cell-types: myeloid cells like macrophages and dendritic cells, innate lymphoid cells (ILC), T regulatory and effector cells (Treg, Teff), and B lymphocytes (Thaiss et al., 2016; Honda and Littman, 2016). The research toolbox available for this dissection entails an inherent tradeoff between tissue structure and the level of control over the experimental parameters. *In vivo* animal models, e.g. the colonization of gnotobiotic mice or the supplementation of conventional mice with bioactive microbes (Hooper et al., 2001), provide physiological tissue structure, but offer poor experimental control. Substantial inter-individual variability, relatively slow timescale of colonization, and difficulty in manipulating the experimental conditions are mostly incompatible with experimental perturbations and real-time readouts. At the other end of the spectrum are *in vitro* culture

systems, in which cell lines or explanted mucosa are grown in monolayers that can be supplemented with microbes (Haller et al., 2000; Tsilingiri et al., 2012), offering tight experimental control but lacking the cellular complexity and architecture. Recent advances in intestinal *in vitro* culture systems include the intestinal organoid culture (Sato et al., 2009; Clevers, 2016), which was developed and is ideally suited to study epithelial development, but lacks the other components, notably immunocytes. An exciting advance is the ‘gut-on-a-chip’ device with separated compartments that can be seeded with different components, including microbes, to study cross-talk between cell-types during the response to microbes (Kim et al., 2016; Kim et al., 2012). However, normal architecture and inter-cellular connections are not preserved in such systems, which also involve cells other than normal gut-resident cells (e.g. cell lines or PBMCs).

Thus, there is a compelling need for an organ culture system that preserves normal differentiated cell-types and their intricate connections in the host yet allows the tight control over experimental conditions and perturbations characteristic of *in vitro* systems. Reasoning that the intestines, themselves, would provide the best source of relevant cells and micro-architectures, we developed a microfluidic system that supports organ intestinal tissue culture, allowing the dissection of host-microbe interaction in a highly controlled fashion *ex-vivo* and with high temporal resolution. The system is multiplexed and enables several cultures to be run in parallel, in order to test experimental inputs under comparable conditions.

Using this system, we demonstrate that intestinal colonization by symbiotic microbes triggers a rapid transcriptional response from the local intestinal tissue, which precedes the long-term immunologic effects induced by these microbes. Comfortingly,

some of these effects overlap with previously described response to particular microbes, but others point to a highly unexpected involvement of the nervous system in sensing and discriminating between intestinal symbionts.

## RESULTS

### *Development of an ex-vivo organ culture system for the gut*

We aimed to implement a three-dimensional gut organ culture system with three main requirements: (i) include all stromal and hematopoietic components of the normal gut, (ii) allow controlled and anatomically valid exposure to microbes, and (iii) allow integrated analysis of the cell biological, biochemical and genomic events elicited by these interactions. These stipulations differed from the motivations behind the existing organoid (Sato et al., 2009), monolayer (Haller et al., 2000), or microfluidic (Kim et al., 2016) *in vitro* systems, whose architectures are not ideally suited to these questions.

Our initial attempts were inspired by fetal thymic organ cultures (FTOC) (Jenkinson and Anderson, 1994), which have proven invaluable in elucidating T cell differentiation in the thymus. Fetal tissue offered a sterile starting point, and culture at the air-liquid interface provided improved oxygen delivery. Unfortunately, organ culture of small fragments of the small or large intestine from perinatal mice at the air-medium interface resulted in collapse of the intestinal lumen, and rapid loss of architecture of the mucosa. We reasoned that maintaining some degree of pressure and flow in the lumen was important, and so designed the Polydimethylsiloxane (PMDS)-based culture unit schematized in Fig. 1A (full description in Fig. S1, Supplementary Methods and Movie S1), which can support the *ex-vivo* culture of sizeable intestinal fragments (~3-4 cm length). The basic unit has two paired inputs and outputs. The first is connected to the intestinal lumen (the gut fragment being threaded and fixed with a surgical thread over the ports) and allows controlled introduction of molecules or microbes into the lumen.

The second enables the introduction and continuous replenishment of medium to support viability of the cultured tissue. This configuration maintains the physiologic separation between the two distinct intestinal environments – the gut lumen (heavily colonized by the microbiota and mostly anaerobic) and the tissue (sterile and well oxygenated). As in FTOC, the tissue is not completely submerged in the external medium, which keeps it from collapsing and, by recapitulating the air-liquid interface principle, allows oxygenation and pH control from an air/O<sub>2</sub>/CO<sub>2</sub> mix injected into the closed chamber. The complete device includes six such chambers for parallel comparison of treatments and conditions. Four multiplexed syringe pumps for regulate inputs and outputs, and a heating block maintains temperature.

In practice, the system can be used to culture colon or small intestine (SI) segments from day18 prenatal to 14 day-old, pre-weaning mice. A number of experiments were performed to optimize the operational parameters: medium composition, oxygenation, addition of specific growth factors (detailed in Supplementary Procedures), leading to the results illustrated for colon cultures in Fig. 1 and Fig. S3, which demonstrate that the tissue remained viable and responsive during the culture period (data for SI cultures in Fig. S2). Standard histological analysis revealed that the overall structure of the cultured tissue was preserved, and that the intestinal epithelial cell (IEC) layer remained intact (Fig. 1B). Although cultures did remain viable for several days, those continued longer than 24 hrs exhibited some epithelial degradation. Consequently, we have conservatively used the system for experiments lasting < 24 hrs. Periodic acid-Schiff (PAS) staining, as well as anti-Mucin2 antibodies, detected mucus-filled goblet cells throughout the colon and a mucus layer in the lumen, although the amount of mucus inside the goblet cells did

decrease by 24 hrs (Fig. 1B/C; Fig. S3A for 0-24h histology). Immunostaining for E-cadherin and Cytokeratin-18 validated the integrity of the intestinal epithelial layer, and Ki-67 staining detected continued proliferation of IEC in the colonic crypts (Figs. 1C/D, S3). Immunostaining for Chromogranin-A, a marker of enteroendocrine cells, showed that these cells remained in proper frequency and location in the colonic epithelium (Fig. 1D, Fig. S3C). Similarly, whole-mount tissue staining for the neural markers Tuj1 and nNOS demonstrated that the enteric nervous system (ENS) structure and spatial organization were maintained in the cultured tissue (Fig. 1E, Fig. S3B, MovieS2). Notably, the cultured tissues exhibited spontaneous peristaltic-like contractions, at least during the first 8 hrs, indicating viability of the intestinal smooth muscle layer and enteric nervous system (MovieS3 (colon), MovieS4 (SI)).

We next verified that the cultures faithfully preserved the immunocyte component of normal intestines. Lamina propria cells from fresh or cultured intestinal tissues were stained for cellular markers of the major lymphoid and myeloid populations (Fig. 2A). Cells in these lineages were readily identified and showed the expected profiles and frequencies throughout the first 24h of culture. We observed only a mild decrease in the proportions of colonic CD11b+CD103+ dendritic cells (fluctuations in monocyte levels were likely due to higher variability in their proportion in input segments). The spatial organization of tissue immunocytes was maintained, as revealed by immunohistochemistry for several markers (illustrated for CX3CR1 in Fig. 2B).

The system was designed to be compatible with time-lapse microscopy imaging. In pilot experiments we cultured gut tissues from (CX3CR1-GFP x CD4-tdTomato) mice ((Jung et al., 2000) and JFM, unpublished) and tracked immunocyte movement (Movie

S5). Peristaltic activity confounded slightly the observation and required immobilization of the segment, but typical movement of T cells was observed in lateral segments of the tissue (in the areas less compressed by the immobilization). Some T cells exhibited complete arrest, forming stable contacts with antigen presenting cells (APCs), while others exhibited active migration through the tissue, sampling many APCs through transient contacts. These and the above results indicate that this organ culture system correctly maintains during the period the structure, cellular composition, and dynamic cell-cell interactions found within the complexity of intact tissues.

We then asked whether intestinal symbionts could be introduced and viably maintained in the cultured gut lumen. With colonic segments from mice housed in a standard Specific Pathogen Free (SPF) facility, the heterogenous bacteria normally present were greatly reduced by gently flushing the colon content during fragment preparation (Fig. 2C). Bacterial titers remained moderate in the first hours, but grew to physiological concentrations ( $\sim 10^9$ CFU/gr) by 24hrs (while the outer medium remained free of contamination). Importantly, these microbes included both anaerobic and aerobic microbes, indicating that conditions in the cultures were favorable to both. In contrast, organ cultures set up from GF donors contained no microbes (Fig. 2D), indicating that contamination was not an issue. To expose the cultures to a defined microbe, we added freshly grown microbes to the medium flowing through the lumen (usually at  $10^7$  CFU/ml). In short-term experiments, this introduced microbe represented the exclusive (when in GF gut segments) or the main (when in SPF segments) microbial exposure, and persisted through the experiment (as illustrated for the strict anaerobe *C. ramosum* in Fig.

2E). With longer times in culture the introduced microbes expanded, and input concentration was adapted accordingly.

Taken together, these results indicate that the gut culture system could support the survival and growth of anaerobic and aerobic microbiota, and facilitate *ex-vivo* colonization of the cultured intestinal tissues with selected exogenous microbes, in a well controlled fashion.

### ***Colonization with SFB triggers a rapid transcriptional host response***

With this system in hand, we analyzed the initial events after exposure to two different microbes known to elicit specific responses in the intestinal immune system. The first was Segmented Filamentous Bacteria (SFB), which induces Th17 cell differentiation in the small intestine (Ivanov et al., 2009; Lecuyer et al., 2014), most likely via multiple steps of intercellular communication involving epithelial and myeloid cells, as well as innate-like lymphocytes (Sano et al., 2015; Atarashi et al., 2015). SFB is very difficult to grow *in vitro* (Schnupf et al., 2015). It takes some time for SFB to be established by *in vivo* passage, so *in vivo* colonization cannot be used to examine the initial events in a finely time-resolved manner. Thus, we interrogated here the first events of SFB:host interactions in the organ culture system, whose broad cell composition is highly valuable. Segments of SI (ileum) dissected from SFB-negative SPF mice were connected to the gut culture system; SFB was flowed into the lumen as a suspension prepared from fecal pellets of SFB mono-colonized mice (Chung et al., 2012) or of GF mice as controls.

A hallmark of SFB colonization *in vivo* is its adherence to the intestinal epithelium, which is important for its Th17-inducing properties (Lecuyer et al., 2014; Ivanov et al., 2009; Atarashi et al., 2015). Thus, we first evaluated the spatial localization of SFB early after *ex vivo* colonization of intestinal tissue. As shown in Fig. 3A, fluorescence in-situ hybridization (FISH) revealed typical SFB filaments in close association with the SI villi, two hrs after SFB introduction. Furthermore, transmission electron microscopy showed SFB within a few microns of the SI epithelium brush border (Fig. 3B). We then asked whether the early association of SFB with the SI IEC triggered a transcriptional response in the tissue. Gene-expression profiles of whole-tissue samples were generated, in triplicate, two hrs after infusion with SFB. Control cultures were infused with supernatant from feces of GF or *B. fragilis*-colonized mice, the latter serving as a non-Th17-inducing control. As illustrated in Fig. 3C, the changes induced by SFB relative to the GF control were mainly of small amplitude (none greater than 2-fold). To focus the analysis, we superimposed a transcriptional signature of chronic SFB colonization *in vivo* (comparing whole-tissue profiles of ileum from SFB-colonized SPF vs SFB-negative SPF mice (Tan T. ms submitted)). Superimposition of this signature revealed a significant bias in the SFB-infused cultures (Fig. 3C), with over-expression of several of the signature transcripts (*Duox2*, *Duoxa2*, *Il2rg*), but not all of them (e.g. *Saa1/2/3*, *Cd177*, *Ly6d*). The *Il17* family members were not biased, but we did not expect them to be, as the differentiation of Th17 cells induced by SFB occurs in a matter of days, not hours. Similarly, we noted biased expression of many of the transcripts in a related “adhesion signature” induced in epithelial cells by binding of SFB and other Th17-inducing microbes (Atarashi et al., 2015) (Fig. 3D). In contrast, some of the

transcripts induced in our system after SFB colonization were not previously found to be biased *in vivo* (e.g. those encoding the chemokine *Ccl7*, the gap junction protein *Gjb2*, and the secreted glycoprotein *Stc1*) (Fig. 3C). These results identify elements of the early response to SFB, and suggest that some of the transcripts rapidly induced remain elevated during chronic exposure, while others may be more transient.

### ***The early response to the Treg-inducing symbiont C. ramosum***

The second microbe/immune-system interaction we analyzed was the induction of a particular population of RORg<sup>+</sup> Treg cells in the colon by individual bacteria species (Sefik et al., 2015; Ohnmacht et al., 2015). This population develops over a matter of days upon microbial exposure *in vivo*, so the culture system promised new insights into the early events of Treg induction. The human symbiont *C. ramosum*, a potent inducer of colonic Tregs *in vivo* (Sefik et al., 2015), was infused into colon cultures from 12-day-old SPF mice, an age when RORg<sup>+</sup> Tregs are still absent (Sefik et al., 2015). Cultures were harvested at various times, and the early transcriptional response determined by gene-expression profiling of mRNA extracted from the whole tissue. As in the SFB-colonized SI, responses to *C. ramosum* were mild, with few transcripts altered relative to medium-infused controls (44 at a Fold Change of >1.5 and p<0.1 at any one time-point; Table S1). These transcripts were induced in sequence (Fig. 4A), with partial overlap between the timepoints. Several of them also responded to long-term *C. ramosum* colonization *in vivo* (Geva-Zatorsky et al, in revision; e.g. *Taf1d*, *Pla2g12b* and *Naalad11*) or overlapped with the *in vivo* response to SFB (i.e. those encoding the ROS-producers *Duoxa2* and *Duox2*, the anti-microbial lectins *Reg3b* and *Reg3g*). A very early and transient response was

observed for *Slfn3*, which encodes a factor that influences epithelial enterocyte differentiation (Kovalenko et al., 2013) or the epithelial tight junction gene *Cldn4*. Other very suggestive transcripts were *Il22*, an essential mediator of the hematopoietic/epithelial crosstalk (Sano et al., 2015) which likely denotes a fast response of the ILC compartment, the *Il1rn* receptor antagonist of the IL1 family (often the initial indicator of an IL1 response) (Gabay et al., 2010), the EGF-family member Epiregulin (*Ereg*), and *Il1rl1* which encodes the IL-33-receptor (aka ST2).

The Treg-inducing symbiont *C. ramosum* triggers a rapid transcriptional response that appears to emanate from several immune and non-immune cell compartments. To narrow the list of candidates to those that are truly involved in the long-term development of colonic RORg<sup>+</sup> Tregs, we performed parallel cultures with colons from GF mice in which we introduced *C. ramosum* or another microbe that is unable to induce RORg<sup>+</sup> Tregs, *P. magnus* (Sefik et al., 2015). Whole tissue samples were again used for transcriptional profiling, two hrs after colonization. Most of the up- and down-regulated transcripts were shared between *C. ramosum* and *P. magnus* (Fig. 4B), including the most robustly responsive transcripts like the *Reg3* family. However, a more subtle part of this early response was unique to *C. ramosum*. Specifically induced transcripts included those encoding the epithelial tight junction protein *Cldn4*, mentioned above, while transcripts specifically repressed by *C. ramosum* encode the cytokine *Il6*, the chemokine *Ccl7*, the precursor protein of Neurokinin A and Substance P neuropeptides *Tac1*, and the synaptic regulator of neurotransmitter release *Snap25*. The former is very suggestive, albeit in a paradoxical direction, which suggests a complex interplay between *Il6* and RORg<sup>+</sup> Treg

induction: Il6 is actually necessary for the full induction of RORg<sup>+</sup> Tregs ((Ohnmacht et al., 2015) and Fig. S4), but its production is initially shut down by inducing microbes.

Since this approach seemed promising for determining which of the induced transcripts were generic and which were more specific to *C. ramosum*, we tested the response to a broader panel of microbes that induce a range of RORg<sup>+</sup> Tregs proportions *in vivo* (representing different phyla) (Sefik et al., 2015). Gene expression in colon cultures was again profiled after 2 hrs, and we correlated the expression of each transcript across the microbe panel vs the frequency of RORg<sup>+</sup> Tregs in mice monocolonized with the same symbionts (Fig. 4C, data from (Sefik et al., 2015)). The transcripts found at the extreme of the distribution of correlation coefficients confirmed several observations from the single *C. ramosum* / *P. magnus* comparison (Fig. 4C). Fittingly, since *C. ramosum* is a strong RORg<sup>+</sup> Treg inducer, these positively and negatively correlated transcriptional signatures were well separated on a “volcano plot” comparing control- and *C. ramosum*-colonized colon cultures (Fig. 4D, left). But when highlighted on a similar representation of the early effect of the Th17 inducer, SFB, the exact opposite was found: transcripts positively correlated with the microbes’ ability to induce RORg<sup>+</sup> Tregs were mostly repressed by SFB; and the genes negatively correlated with RORg<sup>+</sup> Treg induction were induced by SFB (Fig. 4D, right). This mirror-like image suggests that Treg- and Th17-inducing microbes modulate the same pathways in the host gastrointestinal tract, but in an opposite direction during initial encounter, resulting in opposite Treg/Th17 outcomes in the longer term.

Another striking observation resulted from Gene Ontology analysis of these correlated transcripts: those negatively correlated with *in vivo* RORg<sup>+</sup> Tregs were highly

enriched in neurobiological processes, including synaptic transmission, neurotransmitter transport and secretion, and neuropeptide signaling pathways (Fig. 4E). The positively enriched gene-set showed no evocative enrichment. This over-representation is reminiscent of the presence of *Tac1* and *Snap25* among transcripts repressed by *C. ramosum* in Fig. 4B. Taken together, these data suggest that the long-term microbiota-mediated changes in immunocyte activation or frequency may be foretold by the early changes in colonic gene expression in the organ culture system.

***Differential sensing of microbes by the nervous system correlates with immunologic bias***

The unexpected discovery of neuron-related genes among those repressed by RORg<sup>+</sup>-Treg-inducing microbes suggested that triggering of the enteric nervous system might be an early part of this response. This anti-correlation of expression relative to the GF control was not merely driven by a single microbe species, as illustrated for *Tac1* and *TacR1* (Fig. 5A). As the former encodes the pro-inflammatory nociceptive neuropeptide Substance P, we looked more generally for correlations in the effects of Treg-inducing microbes on expression of both neuropeptides and their receptors (Table S2 based on neuropeptide database [www.neuropeptide.nl](http://www.neuropeptide.nl)). Indeed, both gene families showed a broadly biased negative correlation to colonic RORg<sup>+</sup> Treg differentiation (Fig. 5B/C). Nociceptor sensory neurons specifically detect noxious/injurious stimuli (heat, reactive chemicals, tissue injury). In the gut these include extrinsic nociceptor neurons that innervate from the dorsal root ganglia (DRG) and intrinsic primary afferent neurons of the ENS (Mao et al., 2013). Here, transcripts with a negative correlation to *in vivo*

RORg<sup>+</sup> Treg included some known to be enriched in nociceptor neurons (the voltage-gated sodium channels Nav1.7 (*Scn9a*) and Nav1.9 (*Scn11a*), the mechanosensitive channel Piezo2 (*Fam38b*), and the heat-sensitive ion channels *Trpv2*, *Trpv3* and *Trpv4*) strongly suggesting a neuronal origin of these transcriptional changes (rather than the less abundant enteroendocrine component, which can express some neuronal-associated genes). As nociceptors are an important component of the intestinal nervous system and can respond to microbial stimulation and regulate inflammation (Meseguer et al., 2014; Ochoa-Cortes et al., 2010; Chiu et al., 2013; Riol-Blanco et al., 2014), we interrogated a shorter list of neuropeptides more specifically expressed in nociceptive neurons by mining transcriptional profiling datasets of purified DRG nociceptors (Chiu et al., 2014). This 20-gene signature (Table S2) was even more biased towards negative correlations than the whole neuropeptide gene-set (Fig. 5D; Kolmogorov-Smirnoff D-factor 0.37 vs 0.24). We examined whether this bias in neuropeptide expression also occurred in the early intestinal response to SFB. As seen earlier for the differential distribution of the globally correlated signature (Fig. 4D), SFB and *C. ramosum* elicited opposite effects on genes encoding these nociceptor-specific neuropeptides (Fig. 5E). Indeed, *Tac1* had been previously observed in lists of SFB-induced transcripts (Tan T. ms submitted) (Ivanov et al., 2009). How might this broad down-regulation of nociceptive neuropeptides by Treg-inducing microbes actually occur? Although several of these neuropeptide genes may be active in non-neuronal cell-types such as enteroendocrine cells (Gonzalez-Rey et al., 2007), the breadth of the effects and the panel of neuronal signatures that are regulated (Fig. 4-5) suggested the involvement of sensory neurons in the early response to microbial gastrointestinal colonization. *C. ramosum* might be directly triggering neurons

of the ENS, the only neurons present in the organ cultures as connections to ganglia and central neurons are resected, leading to rapid down regulation of these mRNAs. We thus asked whether sensory neurons could directly respond to these microbes, using action potential generation or increases in intracellular  $\text{Ca}^{2+}$  as readouts. Because gut intrinsic primary afferent neurons from adult mice are technically challenging to isolate and culture, we utilized primary adult DRG sensory neurons as a surrogate, which include nociceptor neurons that innervate the colon and SI (T7-L6 DRG neurons) (Robinson et al., 2004; Tan et al., 2008). First, we tested the electrophysiological response to bacteria by plating primary DRG neuron cultures onto multi-electrode array (MEA) plates (see methods), and analyzing the action potential firing of neurons after addition of microbes. Addition of *C. ramosum* resulted in a pronounced increases in the neuronal firing rate (illustrated for representative electrodes in Fig. 6A), with waveforms typical of true action potentials (Fig. 6A, right). These persisted and even increased throughout the experiment (Fig. 6B). In contrast, equivalent loads of *P. magnus* elicited no such response as shown by analysis of well-wide firing rate (Fig. 6B). Secondly, ratiometric  $\text{Ca}^{2+}$  imaging of neurons after addition of the Treg-inducing *C. ramosum* or the non-inducer *P. magnus* showed a striking difference (Fig. 6C/D). *C. ramosum* triggered a robust neuronal calcium influx (Fig. 6C), which initiated at different times of the 900 sec challenge period (Fig. 6D), and ultimately involved 68% of neurons (average, Fig. 6D). The responding neurons included capsaicin-responding nociceptor neurons as well as other DRG sensory afferents (Fig. 6E). Adding *P. magnus* elicited no such  $\text{Ca}^{2+}$  influx (Fig. 6C-D – most neurons remained active, as indicated by capsaicin- and KCl-induced  $\text{Ca}^{2+}$  influx).

We expanded this analysis to include all Th17/Treg-inducing microbes used above, revealing a clear relationship between the microbes' ability to trigger neuronal activation *in-vitro* and their ability to induce RORg<sup>+</sup> Tregs *in vivo* (Fig. 4C, 6F-G). The correlation held at both ends of the spectrum (*P. magnus* and *A. baumannii* vs *C. ramosum* and *B. ovatus*), while intermediate RORg<sup>+</sup> Treg inducers *B. dorei* and *F. varium* elicited delayed and partial neuronal activation. Because SFB is essentially impossible to grow in culture, we used fecal suspensions prepared from monocolonized mice (Fig. 6G); here again, SFB-harboring fecal suspensions elicited little neuronal activation, compared with suspensions from *C. ramosum* monocolonized feces (Fig. 6G).

Heat killing of the bacteria at 95° C inactivated the activity (not shown), but we found that material secreted by *C. ramosum* potently activated neurons (either as a brief wash of the bacteria in neuronal culture medium, or by filtered supernatant after 30' culture of the bacteria in neuronal medium (Fig. 6H). Thus, gut-innervating sensory neurons can directly detect and respond to members of the intestinal bacteria and their products, with a species-specificity that mirrors the transcriptional responses in the organ culture system, and the induction of RORg<sup>+</sup> Tregs *in vivo*.

This down-regulation of nociceptor neuron neuropeptides by Treg-inducing microbes suggested a possible functional connection between neuronal activation and Treg induction. We tested the hypothesis that Substance P (SP) encoded by *Tac1* might negatively regulate colonic Treg differentiation in two ways: first, we compared the frequency of RORg<sup>+</sup> Treg in the colonic LP of *Tac1*<sup>-/-</sup> mice (Cao et al., 1998) and their *Tac1*-proficient littermates (all housed in SPF conditions that promote high RORg<sup>+</sup> Treg frequencies). There was a modest but consistent increase in the colonic RORg<sup>+</sup> Treg

proportions in *Tac1*<sup>-/-</sup> mice (Fig. 7A, left; paired t-test  $p=0.005$ , for a 1.25-fold increase on average). Conversely, because SP and related neuropeptides are released from dense-core vesicles upon activation of sensory neurons, we fed weanling mice with a diet rich in capsaicin, the active ingredient in chili peppers that activates nociceptor neurons (Caterina et al., 1997). The frequency of RORg<sup>+</sup> Treg in the colonic LP of capsaicin fed mice was significantly lower than siblings fed with control diet (Fig. 7B). Overall these results suggest a functional relationship between neuronal activation and neuropeptide release and the development of colonic RORg<sup>+</sup> Tregs.

## DISCUSSION

We report the development of a three-dimensional organ culture system for gut tissue, that has broad applications. It is based on a modification of classic air-liquid interface cultures, the key change being the introduction of medium flow that is independently controlled outside and inside the lumen, which prevents collapse of the tissue, ensures nutrient access, and allows experimental changes in culture conditions. It enables the culture of large, intact intestinal tissues for *ex-vivo* experimentation. This aspect is the main distinction from existing *in vitro* systems, as physiologic cellular populations and their connections are maintained. This advantage led us to discover some unexpected links between the microbiota and the intestinal immune and nervous systems.

As do simple co-culture systems (Haller et al., 2000), organoid (Sato et al., 2009; Clevers, 2016) or ‘gut-on-a-chip’ devices (Kim et al., 2016; Kim et al., 2012), this gut organ culture system provides full control over the experimental parameters: growth medium composition, trophic factors, time-controlled addition of stimulants or perturbagens, etc. It was particularly valuable to analyze immediate/early responses to bacterial exposure, which cannot be reliably assessed *in vivo* since intestinal colonization proceeds progressively, sometimes on the order of days. These robust and well-defined culture conditions, combined with multiplex culture capability, open the door to many investigations in a variety of fields: host interactions with other residents of the gut lumen (viruses/fungi/parasites), fecal samples of different sources or degree of pathogenicity, effects of drugs, metabolites, food antigens, control of intestinal permeability, etc. These can be read out from the integrated standpoint of different organ systems (immune,

neuronal, epithelial) Finally, we showed in preliminary experiments that the system can be combined with time-lapse microscopy to track the dynamics of cell-cell interactions in real time, and it should even be compatible with application of optogenetic tools.

We should acknowledge the limitations of the system as it stands. One is that it does not support experiments that range over several days, as clear problems with tissue structure became apparent by 30-40 hrs, particularly for the small intestine. Thus. It is really best suited for immediate responses to environmental perturbations. Refinements will likely improve the system in the future (physico-chemical conditions, supply of nutrients, growth factors, etc) but there will always be a time limit to any *in vitro* organ culture, as organismal factors (cell migration, multi-organ communication) are unavoidably lost. Second, experiments with bacteria as input are also limited in time, as overgrowth became clear by ~24 hrs. Third, the system cannot be used with human organs, although cells in organs from humanized mice could be used.

Investigations of the immunological effects of the microbiota are mostly performed *in vivo*, where the development of innate and adaptive immune responses occur over a period of days. Here, we utilized the gut culture system to identify and characterize the responses triggered by microbes over a timeframe of hours, correlating these early events to the long-term *in vivo* effects of the same microbes. Two immune-perturbing microbes were investigated, which elicited responses that differ at several levels. SFB, the classic Th17 inducer, elicited transcriptional responses that overlapped to a large extent with the signatures of long-term *in vivo* colonization. This suggests that SFB may be constantly “re-initiating” its activation process, perhaps by repeated burrowing within the epithelium. In contrast, the RORg<sup>+</sup> Treg inducer, *C. ramosum*, seemed to evoke a

different early response. In addition to some generic responses of the epithelium and myeloid compartments shared with other microbes, an array of neuronal genes (particularly neuropeptides of nociceptive sensory neurons) was repressed, with a distribution across bacterial species that correlated with long-term development of RORg<sup>+</sup> Tregs. The subsequent experiments with neuronal activation by microbes, and with genetic or pharmacologic perturbations *in vivo*, substantiated the relevance of this relationship.

The interest in intestinal neuro-immune interactions and their relations with the microbiota is rapidly increasing (Margolis et al., 2016). Yet, little is known about how nociceptor neurons sense signals from the gut microbiota (Baral et al., 2016). Nociceptor neurons express and can be triggered via Toll-like receptors and formyl peptide receptors (Qi et al., 2011; Chiu et al., 2013; Xu et al., 2015). Here, we observed a fast response of sensory neurons to microbes, cultured or from fecal suspensions. This potential was replicated by bacterial washes or supernatants, implying a soluble factor released by some microbes. Neuronal activation correlated well with the microbes' ability to induce RORg<sup>+</sup> Tregs *in vivo*, across a range of microbial species and phyla, and we propose that recognition of some bacterial products by ENS axonal termini can act as a modulator, or even as an intermediate, in this microbiota-immunocyte crosstalk.

One of the transcripts most repressed by RORg<sup>+</sup> Treg inducing microbes was *Tac1*, which encodes a precursor protein to four neuropeptides of the tachykinin family, including Substance P (SP). SP is secreted mainly upon nociceptor neuron activation, and is involved in various neural and neuro-immunologic processes, including nociception and inflammation (Steinhoff et al., 2014). SP modulates immune cell proliferation, can

diminish IL10 production (Janelsins et al., 2013), and supports Th17 differentiation by inducing pro-inflammatory IL-1 $\beta$  and IL-12/IL-23 cytokine production by monocytes (Cunin et al., 2011). Accordingly, SP is thought to play a pro-inflammatory role in the GI tract, as inhibition of SP signaling ameliorates experimental colitis (Weinstock et al., 2003; Engel et al., 2011). The symmetrical findings in mice fed the SP inducer capsaicin, and in SP-deficient *Tac1*<sup>-/-</sup> knockout mice, which show decreased and increased proportions of RORg<sup>+</sup> Tregs, respectively, are in line with the transcriptional observations *in vitro*. They support a functional scenario in which SP inhibits RORg<sup>+</sup> Treg differentiation: the microbes' differential ability to trigger nociceptor neurons and release SP would be an important component in their ability to induce RORg<sup>+</sup> Tregs. We can only speculate about the mechanism through which this inhibition would take place, but the widespread effects of SP on a variety of immunocytes leaves open the possibility of effects on differentiating T cells themselves, on their partner APCs, or even indirectly via ILCs. Of note, the phenotypes of both *Tac1*<sup>-/-</sup> knockout or capsaicin-fed mice were only partial, indicating that SP is certainly not the sole effector at play. SP may be modulating signals delivered more directly by microbes to immunocytes, e.g. via polysaccharides, or functional redundancy in neuromediators may account for the partial effects.

It is interesting that the Th17-inducer SFB actually stimulated *Tac1* expression, here and in our earlier *in vivo* data. Since Treg and Th17 cells are considered divergent paths of T cell differentiation, shutting down or inducing SP may be an early event that endows microbes with the ability to favor one or the other path of differentiation. It also implies that SFB, and perhaps other microbes that fail to induce RORg<sup>+</sup> Tregs, are not

merely neutral in this respect. We interpret the broad repression of the neuropeptide / neuropeptide receptor geneset by *C. ramosum* and consorts as negative feedback in the face of very strong activation. In this light, the impact of SFB on this gene module may be due to triggering of different pathway(s), for instance by the SAA/IL23R centric pathway (Sano et al., 2015), that would happen to crosstalk to SP; or it may result from milder activation of the same nociceptors, at a lower level that results in activation rather than in repression. Investigations of the molecular and genetic differences between these microbes (*C. ramosum* and *P. magnus* are both classified in the *Clostridiaceae* family) will help in elucidating this neural sensing mechanism.

Future investigations will also determine if there are specific subtypes of gut-intrinsic and extrinsic neurons that detect commensal bacteria through specific receptors. For example, it is tempting to speculate that this differential sensing of the microbiota by DRG afferent neurons might mediate gut-brain axis communications and modulate other whole-organism properties, such as behavior. As investigating the interactions between the enteric nervous system and the microbiota in their natural environment are particularly challenging, we anticipate that the gut organ culture system may further contribute to this emerging field.

In conclusion, the observations reported here resulted from the ability to manipulate *in vitro* an experimental system in which most of the broad range of cells and their interactions were preserved. The wholly unexpected interplay between microbiome, nervous and immune systems were revealed by this unbiased approach, and would have been missed with purified cell-types. While fascinating strides are made with single-cell biology and genomics, integrated approaches still clearly have a place.

## **AUTHOR CONTRIBUTIONS**

Conceptualization, NY, LU, AE, YZ, CB, DM, IMC; Investigation, NY, LU, AE, YZ, NYL, JFM; Writing-Original draft, NY, CB; Writing-Review & Editing, NY, CB, DK, DM, LU, AE, YZ, IMC, DW; Funding Acquisition, CB, DM, DW

## **ACKNOWLEDGMENTS**

We thank Drs. N. Surana, E. Sefik, T. Tan and W. Ebina for microbial strains or insightful discussions, AT. Sherpa, J. Ramos, K. Hattori for help with mice; A. Rhoads, L. Yang, G. Gopalan for help with expression profiling; G. Buruzula, C. Araneo for help with sorting, K. Mills for multi-electrode array, P. Ma for help with whole mount staining, C. Gerard and B. Lu for NK1R-KO mice and C. Laplace for help with graphics. This work was supported by a Sponsored Research Agreement from UCB, the JPB Foundation, a gift from the Howalt family and by NIH grants R37-AI051530 to CB and DM, NIH DP2AT009499 and a Harvard Digestive Disease Center pilot grant to IMC. NY was supported by a Schuyler Pierce Memorial Fellowship. JFM was supported by JDRF Post-Doctoral Fellowship 3-2014-216.

## REFERENCES

- Atarashi, K., Tanoue, T., Ando, M., Kamada, N., Nagano, Y., Narushima, S., Suda, W., Imaoka, A., Setoyama, H., Nagamori, T. et al. (2015). Th17 Cell Induction by Adhesion of Microbes to Intestinal Epithelial Cells. *Cell*. *163*, 367-380.
- Baral, P., Mills, K., Pinho-Ribeiro, F.A., and Chiu, I.M. (2016). Pain and Itch: Beneficial or Harmful to Antimicrobial Defense? *Cell Host Microbe*. *19*, 755-759.
- Cao, Y.Q., Mantyh, P.W., Carlson, E.J., Gillespie, A.M., Epstein, C.J., and Basbaum, A.I. (1998). Primary afferent tachykinins are required to experience moderate to intense pain. *Nature*. *392*, 390-394.
- Caterina, M.J., Schumacher, M.A., Tominaga, M., Rosen, T.A., Levine, J.D., and Julius, D. (1997). The capsaicin receptor: a heat-activated ion channel in the pain pathway. *Nature*. *389*, 816-824.
- Chiu, I.M., Barrett, L.B., Williams, E.K., Strohlic, D.E., Lee, S., Weyer, A.D., Lou, S., Bryman, G.S., Roberson, D.P., Ghasemlou, N. et al. (2014). Transcriptional profiling at whole population and single cell levels reveals somatosensory neuron molecular diversity. *Elife*. *3*.
- Chiu, I.M., Heesters, B.A., Ghasemlou, N., Von Hehn, C.A., Zhao, F., Tran, J., Wainger, B., Strominger, A., Muralidharan, S., Horswill, A.R. et al. (2013). Bacteria activate sensory neurons that modulate pain and inflammation. *Nature*. *501*, 52-57.
- Chung, H., Pamp, S.J., Hill, J.A., Surana, N.K., Edelman, S.M., Troy, E.B., Reading, N.C., Villablanca, E.J., Wang, S., Mora, J.R. et al. (2012). Gut immune maturation depends on colonization with a host-specific microbiota. *Cell*. *149*, 1578-1593.
- Clevers, H. (2016). Modeling Development and Disease with Organoids. *Cell*. *165*, 1586-1597.
- Cunin, P., Caillon, A., Corvaisier, M., Garo, E., Scotet, M., Blanchard, S., Delneste, Y., and Jeannin, P. (2011). The tachykinins substance P and hemokinin-1 favor the generation of human memory Th17 cells by inducing IL-1beta, IL-23, and TNF-like 1A expression by monocytes. *J Immunol*. *186*, 4175-4182.

Engel, M.A., Leffler, A., Niedermirtl, F., Babes, A., Zimmermann, K., Filipovic, M.R., Izydorczyk, I., Eberhardt, M., Kichko, T.I., Mueller-Tribbensee, S.M. et al. (2011). TRPA1 and substance P mediate colitis in mice. *Gastroenterology*. *141*, 1346-1358.

Gabay, C., Lamacchia, C., and Palmer, G. (2010). IL-1 pathways in inflammation and human diseases. *Nat Rev Rheumatol*. *6*, 232-241.

Gonzalez-Rey, E., Chorny, A., and Delgado, M. (2007). Regulation of immune tolerance by anti-inflammatory neuropeptides. *Nat Rev Immunol*. *7*, 52-63.

Haller, D., Bode, C., Hammes, W.P., Pfeifer, A.M., Schiffrin, E.J., and Blum, S. (2000). Non-pathogenic bacteria elicit a differential cytokine response by intestinal epithelial cell/leucocyte co-cultures. *Gut*. *47*, 79-87.

Honda, K. and Littman, D.R. (2016). The microbiota in adaptive immune homeostasis and disease. *Nature*. *535*, 75-84.

Hooper, L.V., Littman, D.R., and Macpherson, A.J. (2012). Interactions between the microbiota and the immune system. *Science*. *336*, 1268-1273.

Hooper, L.V., Wong, M.H., Thelin, A., Hansson, L., Falk, P.G., and Gordon, J.I. (2001). Molecular analysis of commensal host-microbial relationships in the intestine. *Science*. *291*, 881-884.

Ivanov, I.I., Atarashi, K., Manel, N., Brodie, E.L., Shima, T., Karaoz, U., Wei, D., Goldfarb, K.C., Santee, C.A., Lynch, S.V. et al. (2009). Induction of intestinal Th17 cells by segmented filamentous bacteria. *Cell*. *139*, 485-498.

Janelins, B.M., Sumpter, T.L., Tkacheva, O.A., Rojas-Canales, D.M., Erdos, G., Mathers, A.R., Shufesky, W.J., Storkus, W.J., Falo, L.D., Jr., Morelli, A.E. et al. (2013). Neurokinin-1 receptor agonists bias therapeutic dendritic cells to induce type 1 immunity by licensing host dendritic cells to produce IL-12. *Blood*. *121*, 2923-2933.

Jenkinson, E.J. and Anderson, G. (1994). Fetal thymic organ cultures. *Curr. Opin. Immunol*. *6*, 293-297.

Jung, S., Aliberti, J., Graemmel, P., Sunshine, M.J., Kreutzberg, G.W., Sher, A., and Littman, D.R. (2000). Analysis of fractalkine receptor CX(3)CR1 function by targeted deletion and green fluorescent protein reporter gene insertion. *Mol Cell Biol*. *20*, 4106-4114.

Kim, H.J., Huh, D., Hamilton, G., and Ingber, D.E. (2012). Human gut-on-a-chip inhabited by microbial flora that experiences intestinal peristalsis-like motions and flow. *Lab Chip*. *12*, 2165-2174.

Kim, H.J., Li, H., Collins, J.J., and Ingber, D.E. (2016). Contributions of microbiome and mechanical deformation to intestinal bacterial overgrowth and inflammation in a human gut-on-a-chip. *Proc Natl Acad Sci U S A*. *113*, E7-15.

Kovalenko, P.L., Yuan, L., Sun, K., Kunovska, L., Seregin, S., Amalfitano, A., and Basson, M.D. (2013). Regulation of epithelial differentiation in rat intestine by intraluminal delivery of an adenoviral vector or silencing RNA coding for Schlafen 3. *PLoS One*. *8*, e79745.

Lecuyer, E., Rakotobe, S., Lengline-Garnier, H., Lebreton, C., Picard, M., Juste, C., Fritzen, R., Eberl, G., McCoy, K.D., Macpherson, A.J. et al. (2014). Segmented filamentous bacterium uses secondary and tertiary lymphoid tissues to induce gut IgA and specific T helper 17 cell responses. *Immunity*. *40*, 608-620.

Mao, Y.K., Kasper, D.L., Wang, B., Forsythe, P., Bienenstock, J., and Kunze, W.A. (2013). *Bacteroides fragilis* polysaccharide A is necessary and sufficient for acute activation of intestinal sensory neurons. *Nat Commun*. *4*, 1465.

Margolis, K.G., Gershon, M.D., and Bogunovic, M. (2016). Cellular Organization of Neuroimmune Interactions in the Gastrointestinal Tract. *Trends Immunol*. *37*, 487-501.

Meseguer, V., Alpizar, Y.A., Luis, E., Tajada, S., Denlinger, B., Fajardo, O., Manenschijn, J.A., Fernandez-Pena, C., Talavera, A., Kichko, T. et al. (2014). TRPA1 channels mediate acute neurogenic inflammation and pain produced by bacterial endotoxins. *Nat Commun*. *5*, 3125.

Mowat, A.M. and Agace, W.W. (2014). Regional specialization within the intestinal immune system. *Nat. Rev. Immunol*. *14*, 667-685.

Ochoa-Cortes, F., Ramos-Lomas, T., Miranda-Morales, M., Spreadbury, I., Ibeakanma, C., Barajas-Lopez, C., and Vanner, S. (2010). Bacterial cell products signal to mouse colonic nociceptive dorsal root ganglia neurons. *Am. J Physiol Gastrointest. Liver Physiol*. *299*, G723-G732.

Ohnmacht, C., Park, J.H., Cording, S., Wing, J.B., Atarashi, K., Obata, Y., Gaboriau-Routhiau, V., Marques, R., Dulauroy, S., Fedoseeva, M. et al. (2015). The microbiota regulates type 2 immunity through ROR $\gamma^+$  T cells. *Science*. *349*, 989-993.

Ootani, A., Li, X., Sangiorgi, E., Ho, Q.T., Ueno, H., Toda, S., Sugihara, H., Fujimoto, K., Weissman, I.L., Capecchi, M.R., and Kuo, C.J. (2009). Sustained in vitro intestinal epithelial culture within a Wnt-dependent stem cell niche. *Nat Med*. *15*, 701-706.

Qi, J., Buzas, K., Fan, H., Cohen, J.I., Wang, K., Mont, E., Klinman, D., Oppenheim, J.J., and Howard, O.M. (2011). Painful pathways induced by TLR stimulation of dorsal root ganglion neurons. *J Immunol*. *186*, 6417-6426.

Riol-Blanco, L., Ordovas-Montanes, J., Perro, M., Naval, E., Thiriot, A., Alvarez, D., Paust, S., Wood, J.N., and von Andrian, U.H. (2014). Nociceptive sensory neurons drive interleukin-23-mediated psoriasiform skin inflammation. *Nature*. *510*, 157-161.

Robinson, D.R., McNaughton, P.A., Evans, M.L., and Hicks, G.A. (2004). Characterization of the primary spinal afferent innervation of the mouse colon using retrograde labelling. *Neurogastroenterol. Motil.* *16*, 113-124.

Sano, T., Huang, W., Hall, J.A., Yang, Y., Chen, A., Gavzy, S.J., Lee, J.Y., Ziel, J.W., Miraldi, E.R., Domingos, A.I. et al. (2015). An IL-23R/IL-22 Circuit Regulates Epithelial Serum Amyloid A to Promote Local Effector Th17 Responses. *Cell.* *163*, 381-393.

Sato, T., Vries, R.G., Snippert, H.J., van de Wetering, M., Barker, N., Stange, D.E., van Es, J.H., Abo, A., Kujala, P., Peters, P.J. et al. (2009). Single Lgr5 stem cells build crypt-villus structures in vitro without a mesenchymal niche. *Nature.* *459*, 262-265.

Sato, T., Katagiri, K., Gohbara, A., Inoue, K., Ogonuki, N., Ogura, A., Kubota, Y., and Ogawa, T. (2011) In vitro production of functional sperm in cultured neonatal mouse testes. *Nature.* *471*, 504-507.

Schnupf, P., Gaboriau-Routhiau, V., Gros, M., Friedman, R., Moya-Nilges, M., Nigro, G., Cerf-Bensussan, N., and Sansonetti, P.J. (2015). Growth and host interaction of mouse segmented filamentous bacteria in vitro. *Nature.* *520*, 99-103.

Sefik, E., Geva-Zatorsky, N., Oh, S., Konnikova, L., Zemmour, D., McGuire, A.M., Burzyn, D., Ortiz-Lopez, A., Lobera, M., Yang, J. et al. (2015). Individual intestinal symbionts induce a distinct population of ROR $\gamma^+$  regulatory T cells. *Science.* *349*, 993-997.

Steinhoff, M.S., von, M.B., Geppetti, P., Pothoulakis, C., and Bunnett, N.W. (2014). Tachykinins and their receptors: contributions to physiological control and the mechanisms of disease. *Physiol Rev.* *94*, 265-301.

Tan, L.L., Bornstein, J.C., and Anderson, C.R. (2008). Distinct chemical classes of medium-sized transient receptor potential channel vanilloid 1-immunoreactive dorsal root ganglion neurons innervate the adult mouse jejunum and colon. *Neuroscience.* *156*, 334-343.

Thaiss, C.A., Zmora, N., Levy, M., and Elinav, E. (2016). The microbiome and innate immunity. *Nature.* *535*, 65-74.

Tsilingiri, K., Barbosa, T., Penna, G., Caprioli, F., Sonzogni, A., Viale, G., and Rescigno, M. (2012). Probiotic and postbiotic activity in health and disease: comparison on a novel polarised ex-vivo organ culture model. *Gut.* *61*, 1007-1015.

Weinstock, J.V., Blum, A., Metwali, A., Elliott, D., Bunnett, N., and Arsenescu, R. (2003). Substance P regulates Th1-type colitis in IL-10 knockout mice. *J Immunol.* *171*, 3762-3767.

Xu, Z.Z., Kim, Y.H., Bang, S., Zhang, Y., Berta, T., Wang, F., Oh, S.B., and Ji, R.R. (2015). Inhibition of mechanical allodynia in neuropathic pain by TLR5-mediated A-fiber blockade. *Nat Med.* *21*, 1326-1331.



## FIGURE LEGENDS

**Figure 1. Development of an intestinal organ culture system.** (A) Schematics of the system design. Intact intestinal tissue is connected to input and output ports of the chamber (top), pumps controlling medium flow inside the lumen and in the external medium chamber. The entire device (bottom) contains six such chambers. (B) Histological analysis of colon tissue structure (H&E staining), and mucus production (PAS staining), of colon fragments cultured for different times. Data representative of >3 independent experiments. (C-D) Confocal imaging of colon segments cultured for 12h, immunostained for several intestinal differentiation or proliferation (Ki-67) markers. Representative of >3 independent experiments (additional time points in Fig. S3). (E) Whole-mount staining of the enteric nervous system in colon segments cultured for 8h (additional time points in Fig. S3 and MovieS2).

**Figure 2. Intestinal immunocytes and microbiota are maintained in culture.** (A) Representative flow cytometry profiles of colonic LP immunocytes isolated from colon segments from 12-14 days old SPF mice, quantitated below for 4-6 segments at each time point from two independent experiments. (B) Confocal imaging of colon cultures immunostained for the myeloid marker CX3CR1 (see MovieS5 for real time immunocyte dynamics) (C) Bacterial concentration (aerobic and anaerobic) in colon segments (as in A) cultured for different times (gray shading is the range observed in normal colon of SPF mice). (D) Bacterial concentration in cultured colon segments originating from GF mice. (E) *C. ramosum* bacterial concentration in SPF segments infused with *C. ramosum*.

**Figure 3. Mucosal association and rapid transcriptional triggering of typical signature by SFB.** (A-B) SFB associates with the intestinal epithelium after 2 hrs in cultured SI segment visualized by (A) FISH with an SFB-specific probe (red) or (B) electron microscopy. (C-D) Induction of intestinal gene expression by SFB. SI organ cultures were infused with bacteria-containing supernatant of feces from SFB- or *B. fragilis*-monocolonized mice or GF controls, and cultured for 2 hrs before microarray profiling of gene expression in the entire tissue. (C) Changes in gene expression on a “volcano plot” comparing SFB or GF infused cultures. Transcripts up- or down-regulated by SFB in whole SI *in vivo* are highlighted (red and blue, respectively). (D) Bar plot comparing the induction by SFB or *B. fragilis* (log<sub>2</sub> FoldChange) of adhesion-mediated IEC activation signature genes (from (Atarashi et al., 2015)).

**Figure 4. Early colonic response to Treg inducing microbes is enriched in neural genes.** (A) Time course heatmap of changes in whole-tissue gene expression in response to *C. ramosum* in SPF colon cultures (log<sub>2</sub> of FoldChange relative to the mean of medium-infused controls; each column an individual sample). Squares: genes observed as responding to SFB *in vivo* [Tan T. ms submitted and (Atarashi et al., 2015)] or to long-term colonization with *C. ramosum in vivo* (from N. Geva-Zatorsky et al, in revision). (B-E) Gene expression was profiled in colon segments from GF mice cultured and infused with different microbes. (B) Comparison of the 2 hr response to *C. ramosum* or *P. magnus* (FoldChange relative to medium control cultures, mean of triplicates). Common responses are labeled in black, those unique to *C. ramosum* in red or blue. (C) Correlation between transcriptional changes elicited *in vitro* by a panel of microbes and their ability

to induce RORg<sup>+</sup> Tregs *in vivo*. Top left: frequency of colonic RORg<sup>+</sup> Tregs in monocolonized mice (data from (Sefik et al., 2015)); top right: ranked Pearson correlation coefficients, highlighting the 300 transcripts most positively or negatively correlated with colonic RORg<sup>+</sup> Tregs (orange and green, respectively); bottom: heatmap representation of the row-normalized expression of these most-correlated transcripts (**D**) Volcano plot comparing *C. ramosum*-infused to control colon cultures (top) or SFB-infused to control SI cultures (bottom; data from Fig. 3), both highlighted with the 300 transcripts most positively or negatively correlated to RORg<sup>+</sup> Treg frequencies, as defined in C (**E**) GeneOntology (biological process) enriched in these most correlated transcripts.

**Figure 5. Treg-inducing microbes modulate colonic expression of neuropeptides and their receptors.** Further analysis of gene expression in microbe-infused colon segments from Fig. 5. (**A**) Frequency of RORg<sup>+</sup> Tregs in monocolonized mice (x-axis) vs mean expression of *Tac1* (top) and *TacR1* (bottom; encode Substance P and its receptor, respectively) in GF colon segments after 2 hr infusion with the same symbionts (y axis). (**B-D**) Ranked correlation to RORg<sup>+</sup> Treg frequency (per Fig. 4C) highlighted for transcripts encoding neuropeptide receptors (**B**), neuropeptides (**C**) or neuropeptides most expressed in nociceptor neurons (**D**); Kolmogorov-Smirnoff test p-value and D-factor. (**E**) Log2 of FoldChanges vs control for *C. ramosum*-infused colon (red) or SFB-infused SI (blue) for neuropeptides most enriched in nociceptor neurons.

**Figure 6. Differential activation of sensory neurons by RORg+ Treg inducing microbes compared to non-inducers via soluble mediators. (A-B)** Multi-electrode array recordings of cultured dorsal root ganglia (T7-L6 DRG) sensory neurons. **(A)** Individual raster plots of recorded action potentials over time for *C. ramosum* or *P. magnus*; average action potential waveform for each electrode is shown at right. **(B)** Average spike rate comparison following stimulation by *C. ramosum* or *P. magnus* across MEA plates (n=6 per strain; two-way ANOVA p.value). **(C-H)** Mouse dorsal root ganglia (T7-L6 DRG) neurons were analyzed by Fura-2 ratiometric imaging for bacterial responses. Microbes were applied to cultured neurons ( $10^7$ - $10^8$  CFU/mL), followed by capsaicin (Cap) to mark nociceptor neurons, and KCl to activate all sensory neurons in the imaging field. **(C)** Representative fields showing calcium flux in neurons responding to *C. ramosum* (white arrows) but none to *P. magnus*. **(D)** Individual Fura-2 ratiometric traces of neurons showing calcium influx following application of bacteria, capsaicin, and KCl. Right: quantitation of the frequency of neurons responding to the two bacterial strains (response scored if the fold-change increase vs. basal state was  $\geq 1.2$ ; student's t-test p value  $< 10^{-4}$ ). **(E)** Venn diagram of neuronal subsets responding to *C. ramosum*, capsaicin, or both. **(F-H)** Representative Fura-2 ratiometric traces of neurons **(F, left)** and quantitation of the frequency of neurons responding **(F, right)** to 6 different cultured microbes or to fecal suspensions from GF, SFB or *C. ramosum* mono-colonized mice **(G)**. **(H)** Neurons respond to bacterial washoff and supernatant from *C. ramosum* but not from *P. magnus*. Bacterial cultures were washed into neuronal imaging medium for preparation of unconditioned supernatant (left) or incubated for 30min for conditioned supernatant (right).

**Figure 7: *Tac1* deficiency and neuronal activation by capsaicin feeding alters colonic RORg<sup>+</sup> Tregs levels *in-vivo*** (A) Frequency of RORg<sup>+</sup> Tregs among colonic FoxP3<sup>+</sup> Tregs in *Tac1*-deficient mice or control littermates (paired Student's t-test); middle: KO/WT ratio of RORg<sup>+</sup> Treg frequencies in each littermate pair; right: frequency of total colonic FoxP3<sup>+</sup> Tregs. (B) Frequency of RORg<sup>+</sup> Tregs among colonic FoxP3<sup>+</sup> Tregs (left) and total colonic FoxP3<sup>+</sup> Tregs (right) in mice fed with a capsaicin enriched diet vs. control diet (unpaired Student's t-test).

# STAR Methods

## CONTACT FOR REAGENT AND RESOURCE SHARING

Further information may be obtained from the Lead Contact Christophe Benoist (e-mail: [cbdm@hms.harvard.edu](mailto:cbdm@hms.harvard.edu). Address: Division of Immunology, Harvard Medical School, 77 Avenue Louis Pasteur, Boston, MA 02115)

## EXPERIMENTAL MODEL AND SUBJECT DETAILS

### Mice

C57BL/6J (B6), B6.Cg-Tac1tm1Bbm/J (Tac1<sup>-/-</sup>) and B6.129S2-Il6tm1Kopf/J (IL-6<sup>-/-</sup>) mice were obtained from Jackson Laboratory (JAX), NOD/LtJ.DOI from our colony, and all bred in the specific-pathogen-free (SPF) facility at Harvard Medical School (HMS). A germ-free (GF) B6 breeding nucleus was obtained from L. Bry, and maintained in germ-free isolators. GF Swiss-Webster mice and SFB mono-colonized Swiss Webster colony housed in GF isolators at the Kasper lab GF animal facility. For gut organ cultures experiments of SPF housed mice, B6 females were crossed with NOD males, and intestinal tissues were dissected from 12-14 days old F1 littermates. For gut organ cultures of GF mice, 14 days old GF B6 were used. For analysis of colonic Tregs in Tac1<sup>-/-</sup> or IL-6<sup>-/-</sup> mice, B6 female mice were first crossed with Tac1<sup>-/-</sup> or IL-6<sup>-/-</sup> males to obtain F1 heterozygotes, which were intercrossed to generate WT and KO littermates. For capsaicin diet experiments, B6xNOD F1 littermates mice, 14d old, were put on Capsaicin-enriched chow or a vehicle chow, for 12-14 days. Capsaicin was purchased from Tocris (Catalog 0462), and the Capsaicin enriched chow (0.01% Capsaicin added) was prepared by PhamaServ (Framingham, MA) with Pico Rodent 5053 (catalog 56023). All experimentation was performed following animal protocols approved by the HMS Institutional Animal Use and Care Committee (protocols 02954 and IS00000054).

### Bacteria

Bacteria were obtained from the American Type Culture Collection (ATCC), Biodefense and Emerging Infections Research Resources Repository (BEI Resources), Deutsche Sammlung von Mikroorganismen und Zellkulturen (DSMZ). Detailed description of bacteria origin and culture conditions are listed in Table S3. Anaerobic bacteria were cultured on rich medium (Per liter: 20gr proteose peptone, 5gr yeast extract, 5gr NaCl, 5gr glucose, 5gr K<sub>2</sub>HPO<sub>4</sub>, 0.5gr L-cysteine, 5mg

hemi, and 2.5ml vitamin K1) under strictly anaerobic conditions (80% N<sub>2</sub>, 10% H<sub>2</sub>, 10% CO<sub>2</sub>) at 37°C in an anaerobic chamber. For SFB experiments, fresh fecal pellets from SFB mono-associated Swiss-Webster (SW) mice were collected, as well as pellets from GF SW mice, which served as a control. We also used fecal pellets from *B. fragilis* mono-associated B6 mice and GF B6 mice, as a non-Th17 inducing control. Fecal pellets (500-1000mg) were resuspended in 10ml of sterile tissue culture medium, previously incubated in the anaerobic chamber for 48h (medium composition is detailed in the gut culture system methods section). Fecal suspension was left to stand for 5 minutes to allow sedimentation of solids, the supernatant was collected into the input syringes and loaded on the gut culture syringe pumps.

## METHOD DETAILS

### **Ex-vivo gut organ culture system**

Detailed description of the organ gut culture system development, operation and device fabrication is in the supplemental information (as well as video protocol in MovieS1). Briefly, intact whole colons or small-intestinal tissues (ileum) were dissected sterilely from SPF of GF mice (12-14 days old). The solid lumen content was gently flushed, and the gut fragment was threaded and fixed over the luminal input and output ports using a sterile surgical thread. The culture device was placed on a controlled heating block for temperature of 37°C, and tissues were maintained half-soaked in a constant flow of sterile medium using a syringe pump. Anaerobic bacterial cultures were resuspended in de-gassed tissue culture medium and infused into the gut lumen using a syringe pump. Gas outlet in the device lid flow humidified and filtered, medical grade 95% O<sub>2</sub> / 5% CO<sub>2</sub> gas mixture into the device.

### **Gene expression profiling and bioinformatic analysis**

For microarray analysis, a small tissue fragment (~3mm) was dissected into Trizol (Invitrogen), homogenized, and RNA prepared. Profiling was performed on Affymetrix Mouse Gene 1.0 ST arrays as previously described (Sefik et al., 2015). Microarray data were background-corrected and normalized using the robust multi-array average (RMA) algorithm implemented in the GenePattern software package and replicates were averaged. Analysis focused on genes with a mean expression value > 120 in at least one sample with a coefficient of variation < 0.3. Scatter analysis (MultiplotStudio) and hierarchical clustering were performed in GenePattern.

### **Preparation of mice dorsal root ganglia (DRG) neurons culture**

Primary lumbar dorsal root ganglia (DRG, segments T7-L6) from adult mice (7–12 weeks) were dissected into neurobasal-A medium (Life Technologies), dissociated in 1 mg/ml collagenase A plus 2.4 U/ml dispase II (enzymes, Roche Applied Sciences) in HEPES-buffered saline (Sigma) for 70 min at 37°C. After trituration with glass Pasteur pipettes of decreasing size, DRG cells were centrifuged over a 10% BSA gradient, plated on laminin-coated cell culture dishes in B27 supplemented neurobasal-A medium plus 50 ng/ml nerve growth factor (NGF) plus penicillin/streptomycin (Life Technologies).

### **Real-time calcium imaging of live DRG neurons and image analysis**

DRG neurons were used for calcium imaging 16–24h after plating. Cells were loaded with 10 mM Fura-2-AM (Life Technologies) at 37°C for 30 min in neurobasal-A medium, washed into Krebs Ringer Buffer, and imaged at room temperature. Neuronal calcium imaging was performed using an inverted Nikon Ti-S microscope equipped with a Lambda XL light source and NIS-elements software (Nikon). Cells were illuminated by an ultraviolet light source (Xenon lamp, 75 W, Nikon), 340 nm and 380 nm excitation alternated by a LEP MAC 5000 filter wheel (Spectra services), and fluorescence emission captured by Cool SNAP ES camera (Princeton Instruments). 340/380 ratiometric images were processed, background corrected, and analyzed with NIS Elements (Nikon). Microsoft Excel was used for further analyses. Microbes were cultured on Brucella Blood agar plates in an anaerobic incubator for 48h prior to experiment, scraped from the plates, resuspended in Krebs Ringer solution on ice, and bath applied few seconds after the beginning of imaging at  $10^{8\pm 1}$  CFU/mL. Microbial density was determined by OD<sub>600nm</sub> (using a pre-determined OD/CFU calibration curve) and validated by microbial growth and colonies counting. For co-culture experiments using fecal samples, bacterial suspensions were prepared in Krebs Ringer solution, as described above (see 'Bacteria' section). For bacterial supernatant experiments, neural cultures were supplemented with bacterial supernatant prepared from conditioned or unconditioned medium (bacterial 'wash'). For preparation of bacterial conditioned supernatant, bacteria were cultured on rich medium in anaerobic conditions, spin down and transferred to Krebs Ringer Buffer, and cultured for 30 minutes in anaerobic incubator. The medium was then centrifuged at 12,000rpm for 10 minutes, and the supernatant was filtered through a 0.22µm filter, and added to the neurons cultures during imaging. For preparation of bacterial unconditioned supernatant ('wash'), microbes were scraped from the Brucella Blood agar plates and resuspended in Krebs Ringer Buffer. The medium was then centrifuged and the supernatant was filtered, and added to the neuron cultures. 1 mM capsaicin (Tocris) and or 40mM KCl (Sigma) were applied after bacterial ligands to control for responsiveness of the neurons. Neuronal responses to each type of stimuli were counted for each field of cells by a blinded observer.

### **Electrophysiology using Micro-Electrode Array (MEA) and data analysis**

For multi-electrode arrays, DRG neurons were isolated as described above and plated on MEA 64-electrode probes plates at 30,000 cells/plate (Axion BioSystems). Cells were grown in Neurobasal-A medium plus B27, 50 ng/mL NGF (Life Technologies), and 1  $\mu$ M Ara-C (Sigma). 7 days after plating, the Axion Muse device was used to record neuronal activity. Neurons were recorded in Neurobasal medium at 37°C. Microbes were centrifuged, resuspended in Neurobasal medium, and added at  $10^{8\pm 1}$  CFU/mL to neurons. Spikes were identified using thresholding by Axion's Integrated Studio (AsIS) software across all electrodes, and spike files exported for further data analysis in Excel (Microsoft). Action potential waveforms were extracted using neuroexplorer (Neuroexplorer).

### **Lymphocytes and flow cytometry**

Intestinal tissues were treated with RPMI containing 1 mM DTT, 20 mM EDTA and 2% FBS at 37°C for 10 min to remove epithelial cells, minced and dissociated in collagenase solution (1.5mg/ml collagenase II (Gibco), 0.5mg/ml dispase and 1% FBS in RPMI) with constant stirring at 37°C for 30min. Single cell suspensions were then filtered and washed with 4% RPMI solution. Spleens were mechanically disrupted. Single-cell suspensions were stained with antibodies against mouse CD4, CD8, TCR- $\beta$ , TCR- $\gamma\delta$ , CD45, CD19, CD11b, CD11c, Ly6c, F4/80, CD103, Helios (Biolegend), ROR $\gamma$  and FoxP3 (eBioscience). For intracellular staining of transcription factors, cells were stained for surface markers and fixed in eBioscience Fix/Perm buffer overnight, followed by permeabilization in eBioscience permeabilization buffer for 45 min in the presence of antibodies. Cells were analyzed with a BD LSRII flow cytometer, and data processed with FlowJo (Tree Star) software.

### **Histology, immune-fluorescence staining and confocal microscopy**

For histological analysis, tissues were fixed in Carnoy's fixative (Electron Microscopy Sciences) to preserve the mucus layer. Tissues were embedded in paraffin, sectioned and stained with Hematoxylin and Eosin or Periodic Acid-Schiff.

For immune-fluorescence, intestinal tissues were embedded in OCT, fresh frozen and stored in -80°C. Frozen tissues were sliced using microtome to 7 $\mu$ m thick sections and fixed in cold acetone for 10 minutes. Tissues were washed twice in PBS (20min) and blocked with serum (10% in PBS) of the same species as the secondary antibody for 1h at room temperature. Tissue sections were then rinsed in staining buffer (1% BSA, 0.3% Tween-20 in PBS), and incubated with primary antibody, diluted 1:100 in blocking solution, for 1h at room temperature or over night at 4°C (anti-Mucin2 sc-15334 and anti-Cyt-18 sc-51582; Santa-Cruz Biotechnology); anti-Ecadherin (CD324, cat:147302, BioLegend); anti-Ki-67 (cat:556003, BD Biosciences); anti-CX3CR1 (cat:824001,

BioLegend); anti-Chromogranin-A (cat: ab15160, AbCam). Tissue sections were then wash 3 times with staining buffer and incubated with secondary antibody (Cy3 or Cy5-conjugated donkey anti-rabbit/rat/mouse, Jackson Laboratories) for 1h at room temperature. After washing, sections were counterstained with DAPI (1ug/ml) for nuclear visualization, and mounted with Fluoromount-G mounting medium (SouthernBiotech, Cat No. 0100-01). Images were acquired on an Olympus Fluoview Confocal microscope.

For whole-mount staining of the enteric nervous system, freshly-dissected or cultured colons were immersed on ice for 20mins in 1uM nifedipine hydrochloride (calcium channel blocker) to maximize smooth muscle relaxation. Tissues were cut open longitudinally, and stretched out and pin flat on Sylgard-lined plates. Tissues were fixed with 4% PFA for 1 hour on ice, and permeabilized with 0.1% Triton X-100 in DPBS for 2 hours with gentle shaking at room temperature. Samples were blocked with 10% donkey serum / 0.1% Triton X-100 / DPBS for 1 hour with gentle shaking at room temperature, and then incubated with 1:100 goat anti-nNOS (Abcam 1376, final 5ug/ml) and 1:1000 rabbit anti-Tubulin beta-3 (Biolegend 802001, final 1ug/ml) in blocking buffer (10% donkey serum / 0.1% Triton X-100 / DPBS) overnight at 4°C. Samples were washed in DPBS for 10 minutes at room temperature, 3 times, and incubated with 1:200 secondary antibodies (Jackson, donkey anti-goat Cy5, and donkey anti-rabbit Cy3, final 7.5ug/ml) in blocking buffer for 1 hour at room temperature. Samples were washed 3 times, incubated in 1:2000 Hoechst in DPBS (final 5ug/ml) for 15 minutes at room temperature, washed again and then mounted on slides with mounting media. Z-stack images were acquired on an Olympus Fluoview Confocal microscope (1um intervals), and 3D images were reconstructed using Imaris.

For live imaging experiments, we made two change to the standard gut culture protocol: 1- the culture medium was free of phenol red, to improve imaging. 2- the PDMS slabs were bonded to a thin cover glass slide (no. 1 thickness, 75 mm x 50 mm, Brain Research Laboratories), instead of the regular 1mm thick glass slide. Colons were dissected from CX3CR1-GFP x CD4-RFP double transgenic mice, and connected to the gut organ culture device. The device was then placed on a heated microscope stage (medium temperature of 37c), and supplemented with gas mixture of 5% CO<sub>2</sub> and 95% O<sub>2</sub>. A 20x objective was used for imaging. To minimize peristalsis, colon tissues were held against the coverslip during acquisition, using a small piece of Tputty material (Laird Technologies) and slight pressure. To create time-lapse sequences, we scanned individual Z-stacks at a 40 second interval, containing 11 optical sections with step size of 3 um between sections, on an Olympus FV1000 confocal microscope. Image acquisition was initiated after a 5 hour period of ex-vivo organ culture and each individual imaging run was typically 30-45 minutes in duration. 3D reconstructions of raw imaging data were generated using Imaris software (Bitplane) to evaluate cellular migration patterns and interactions between individual cells.

### **Bacterial Fluorescence In-Situ Hybridization (FISH)**

Intestinal tissues were fixed with Carnoy's fixative (Electron Microscopy Sciences, cat:64130-50) at room temperature. Tissues were embedded in paraffin, sectioned, dewaxed using EZ-DeWax solution (BioGenex), 3 times for 5 minutes at room temperature, and washed with reagent-grade ethanol (Sigma) between incubations. Tissue sections were then washed with pre-warmed (50°C) hybridization solution (20 mM Tris-HCl, pH 7.4, 0.9M NaCl, 0.1% SDS)). The hybridization step was performed at 50°C overnight with a Cy-5 or Alexa-568 conjugated EUB338 probe (5'-GCTGCCTCCCGTAGGAGT-3'), and Alexa-488 conjugated SFB probe (5'-GGGTACTTATTGCGTTTGCACGGCAC-3'), diluted to a final concentration of 10µg/ml in hybridization buffer. Sectioned were washed 3 times with pre-warmed hybridization buffer, stained by standard DAPI staining and mounted with Fluoromount-G.

### **Transmission electron microscopy**

For transmission electron microscopy analysis, tissues were fixed in 2.5% Glutaraldehyde 1.25% Paraformaldehyde and 0.03% picric acid in 0.1 M sodium cacodylate buffer (pH 7.4). Small tissue pieces (1-2mm cubes) were fixed for at least 2 hours at RT in the above fixative, washed in 0.1M cacodylate buffer and postfixed with 1% Osmium tetroxide (OsO<sub>4</sub>)/1.5% Potassium ferrocyanide (K<sub>4</sub>Fe(CN)<sub>6</sub>) for 1 hour, washed in water 3x and incubated in 1% aqueous uranyl acetate for 1hr followed by 2 washes in water and subsequent dehydration in grades of alcohol (10min each; 50%, 70%, 90%, 2x10min 100%). The samples were then put in propyleneoxide for 1 hr and infiltrated ON in a 1:1 mixture of propyleneoxide and TAAB Epon (Marivac Canada Inc. St. Laurent, Canada). The following day the samples were embedded in TAAB Epon and polymerized at 60°C for 48 hrs. Ultrathin sections (~60nm) were cut on a Reichert Ultracut-S microtome, picked up on to copper grids stained with lead citrate and examined in a JEOL 1200EX Transmission electron microscope or a TecnaiG<sup>2</sup> Spirit BioTWIN and images were recorded with an AMT 2k CCD camera.

## **QUANTIFICATION AND STATISTICAL ANALYSIS**

Statistical parameters including the definition and exact values of n, distribution and deviation are reported in the figures and corresponding legends. Most data are represented as mean ± SEM using Student's t tests. Statistical analyses were performed in Microsoft Excel and GraphPad Prism.

## DATA AND SOFTWARE AVAILABILITY

The accession number for the microarray data reported in this paper is NCBI GEO: GSE92471.

## ADDITIONAL RESOURCES

### Detailed description of the Gut Organ Culture device

#### **Gut culture fluidic system, design and fabrication**

We created a device for three-dimensional intestinal organ culture and experimentation, whose use is detailed in the accompanying protocol and video (Movie S1). The custom-fabricated fluidic chip holds up to six individual gut tissue fragments in isolated chambers. Each chamber is 8 mm wide and 25 mm long to accommodate mouse gut fragments of varying sizes and to provide a bath of nutrients (Fig. S1). The nutrient rich environment created by sealing the fluidic chip with a lid to maintain an O<sub>2</sub>/CO<sub>2</sub>-rich atmosphere and to prevent outside contaminants from entering the system. The lid is patterned so that it precisely matches the outer dimensions of the fluidic chip (75 mm by 33 mm; Fig. S1). Both the chip and the lid are made from poly(dimethylsiloxane) (PDMS; Sylgard 184, Dow Corning, Midland, MI) by replica molding of a 3D printed master (Xia & Whitesides, 1998). The masters were designed using AutoCAD (Autodesk, Inc., San Rafael, CA) and printed using veroBlue on an Object 30 3D printer (Stratasys Ltd., Eden Prairie, MN; the AutoCad design file and 3D printing instructions were deposit at GitHub.com). The masters are baked overnight in an oven at 90°C to

fully cure the material. Each master consists of a patterned base and a frame. The frame is assembled around the base prior to molding, then PDMS base and cross-linker are mixed together in a 10:1 ratio and poured into the mold. The PDMS is de-gassed in a vacuum chamber for 30 minutes to remove air bubbles, then the filled molds are placed in the oven overnight at 55°C until the PDMS is fully cured. The solid PDMS slabs can be removed from the molds by lifting out the frame, then gently removing the PDMS from the mold by the edges. The PDMS slabs are bonded to a glass slide (Corning, 75 mm x 50 mm) using all-purpose sealant (100% silicone sealant, DAP Products, Inc., Baltimore, MD) and cured overnight at room temperature. These slides form the top and bottom of the device. Four fluidic connections are made to each chamber (two inputs, two outputs) at the appropriate locations with a needle (input/output ports were aligned to the middle section of each channel described in Fig. S1, ~3mm high). Holes blunt needles (1.5” long) threaded through holes previously punched: 22G needles (McMaster-Carr, Cleveland, OH) are used to provide flow to the intestinal lumen, and 18G needles (McMaster-Carr) are used to connect to the outer medium chamber. The area around each needle is also sealed with silicone sealant and left to cure overnight. Surgical thread, which will be used later to secure the gut segments in place, is knotted around the luminal input and output ports. The entire system is sterilized by dry-cycle autoclaving at 121°C for 20 minutes.

### **Gut culture fluidic system, set up**

To control the flow inside the lumen and in the external medium for each chamber on the device, the input and output ports are connected to a set of four multiplex syringe

pumps capable of infusion and aspiration of fluid from six syringes in parallel (NE-1600, New Era Pump Systems, Inc., Farmingdale, NY). Thus, the first pump is loaded with six syringes, each for every gut fragment, and flows the lumen content into the input ports. Similarly, the second pump flows the external growth medium, and the last two pumps drain these inputs, respectively (Fig. 1A). Each syringe is connected to the device with Tygon PVC tubing (ID: 1/16", OD: 1/8"; McMaster-Carr) and a Luer lock to barbed tubing adaptor (1/16" sockets; McMaster-Carr). Prior to use, the tubing and adaptors were also sterilized using an autoclave.

During a culture experiment, the temperature of the device is maintained at 37°C using a standard lab hot plate, set to 43°C (for 37°C inside the culture device, see optimization experiments below). A heat spreader was made using 1/8" copper and placed on the hot plate. The copper heat spreader serve as an adapter between the hot plate and the culture device, and allows fixing the culture device in place by screwing a plastic lid over the device (see Movie S1). The fluidic device is placed directly onto the copper heat spreader with a layer of heat-sink silicon compound (Chemplex 1381 DE, Lubritech), to ensure optimal heat transfer.

A medical grade mixture of 5% CO<sub>2</sub> and 95% O<sub>2</sub> is provided to the device from a compressed gas cylinder connected to a regulator. The flow from the regulator is connected to the device lid through a 14G flat-end needle and Luer lock tubing adaptor. Additional 20G needle was added in the opposite side of the lid, for pressure release. The gases are humidified (using standard oxygen humidifier) and filtered through a 0.22µm syringe filter (EMD Millipore).

## **Gut culture fluidic system, operation**

All culture preparations and tissue dissections were done in a biological hood to maintain sterility. Prior to dissection, input/output ports were flushed using sterile culture medium, and the gut culture device was washed and filled with culture medium. Intact whole colons or small-intestine (ileum) were dissected sterilely from SPF or GF mice (commonly from 12-14 day-old mice). The solid lumen content was gently flushed, the gut fragment was washed in sterile medium, and then threaded and fixed over the luminal input and output ports using the pre-positioned surgical thread (Fig. 1A, see video tutorial at Movie S1). The culture device (sealed using the fabricated lid) is placed on the heat-conducting copper adaptor, on a layer of heat-sink silicon compound (CHEMPLEX 1381 DE, Lubritech). The serum-free tissue culture medium contains Iscove's Modified Dulbecco's Medium (IMDM, Gibco) supplemented with 20% KnockOut serum replacement (Gibco), 2% B-27 and 1% of N-2 supplements (Gibco), 1% L-glutamine, 1% non-essential amino acids, 1% HEPES. The tissue culture medium was loaded into 10ml syringe (for short-term experiments, or 30ml syringes for 24h experiments) and infused into the device input ports by a syringe pump (flow rate of 1ml/h). To infuse bacteria, bacterial cultures were resuspended in de-gassed tissue culture medium (incubated for 48h in the anaerobic chamber, in a filtered bottle), loaded into 5ml syringes and infused into the colon lumen by a syringe pump (flow rate of 30 $\mu$ l/h).

## **Testing and Optimization of the Gut Organ Culture device**

We performed numerous development and optimization experiments that precede the finalized gut organ culture protocol presented in the main text. Detailed below are

many of these trial and error experiments, which might be useful for future adaptations and modifications of the system.

Gut culture device:

We tested a protocol for culture of intestinal sphere-like organoids in a collagen gel with an air-liquid interface, previously reported by Ootani et al (2009). While recapitulating this protocol was successful, we could not utilize the same approach to culture large, intact, intestinal fragments dissected from embryonic (E19) or newborn (day 1-2) mice. Culture of these large tissue fragments embedded in the collagen gel matrix resulted in tissue damage and loss of tissue shape, color and integrity.

We performed preliminary experiments aiming to culture intestinal tissues inside a glass capillary, with medium flow around the tissue and lumen connection into the lumen. However, we could not properly separate the inside luminal flow from the outside medium. Also we could not supply proper oxygen diffusion to the tissue.

We tested the classical air-liquid interface approach, as recently utilized by Sato et al (2011) to culture neonatal mouse testes. We followed this protocol for culture of embryonic (E19) and newborn (day 1-2) intestinal tissue fragments (2-3cm long). Surprisingly, most of the intestinal tissues seemed viable, and showed spontaneous peristalsis-like contractions lasting for days and in few occasions up to 3 weeks. Additionally, these tissues showed positive CD45 staining when tested during the first 3 days in culture. However, this simple air-liquid interface approach of intestinal organ cultures resulted in collapse of the intestinal lumen, and rapid loss of architecture of the mucosa. We made few improvements to address these issues. First, we created a channel-

like structure in the agarose bedding that is filled with culture medium and enables the tissue to ‘float’ during cultures and prevent tissue collapse. Second, we connected the gut fragments to a micro-tube and a syringe pump, to maintain flow and positive luminal pressure. These improvements resulted in an improved maintenance of the cultured gut tissue structure, as evaluated by standard histology. Yet, additional requirements led us to further develop the current gut culture device: 1- establish the organ cultures outside of the standard tissue culture incubator, to support convenient connections to pumps, real-time readout and manipulation, and oxygen enrichment. 2 – robust culturing platform that allows precise control over the medium flow, and multiplexing capability of multiple gut cultures in the same experiment. 3- support the culture of larger tissues dissected from older mice (in addition to the embryonic tissue cultures tested in the air-liquid interface method). We addressed these issues by developing the PDMS-based gut organ culture device described in the main text.

#### Medium composition:

Preliminary experiments were performed according to previously published protocols, mostly using fetal calf serum based medium, supplemented with growth factors (i.e., Ootani et. al., 2009). To increase experiments reproducibility and support standardization, we developed a serum-free culture medium, based on the KnockOut serum replacement (KSR, Invitrogen) and supplements to support the different cellular populations in the tissue (stem cells, neurons, immune cells, etc... See above full description of medium composition). Additional growth factors tested during the optimization phase, but were not included in the final medium formulation, include EGF

(50-500ng/ml), R-spondin1 (500ng-5ug/ml), Amphiregulin (5ug/ml). We also tested AlboMAX (Invitrogen), Prostaglandin E2, Nicotinamide, Dexamethasone, Sodium pyruvate and beta-mercaptoethanol. These factors were eventually not used in this study, as we did not observe any visible change to overall tissue structure or viability.

#### Gas flow:

Preliminary experiments were performed in a standard tissue culture incubator, with 5% CO<sub>2</sub> and no additional oxygen. In the gut culture device, we tested the effect of oxygen enrichment on tissue structure using standard histology. We found that oxygen enrichment improve tissue viability, and facilitate the culture of larger intestinal fragments. Thus, the final settings include a constant flow of medical grade mixture of 95% O<sub>2</sub> and 5% CO<sub>2</sub> (to maintain pH of the culture medium) into the device. The gas mixture was humidified (using standard oxygen humidifier) and filtered through a 0.22um syringe filter (EMD Millipore).

#### Tissue source:

The classical air liquid interface method described above supported the culture of intestinal fragments dissected from mice embryos of neonates (E19 to P1-2). The current gut culture device, however, also enables the culture of larger intestinal fragments, dissected from mice at pre-weaning stage (14 days old), as described in the main text. Culture of embryonic tissues in the gut culture device supplies a sterile starting point for microbial colonization. This requires adapting the input and output port size to this smaller tissue size, thus replacing the 22G flat-end needles with 30G ones.

Fluid control and medium flow rate:

We compared medium flow by gravity, from a reservoir placed above the tissues, to flow infusion controlled by syringe pump. Although gravity-based flow did not require purchase of special equipment, it was very difficult to control the input flow rate and output draining. We also tested medium infusion to multiple gut fragments using pump with one syringe, where the tubing is then split to multiple tissues. We found that the luminal flow resistance in one tissue affected the flow rate in the other tissues. We thus used syringe pumps capable of controlling multiple syringes (one syringe per one tissue), for both input (infusion) and output (withdrawal). This create a 'closed system' which allows individual control of luminal flow of each tissue fragment, and allows the collection of the culture medium in real-time for individual gut cultures.

We tested different flow rates of the external and internal culture medium. For the external medium, flow rate should be high enough to replenish nutrients, maintain pH and compensate for mild evaporation. We found that flow rate of 200-500ul/h was too slow to fill these requirements, thus the external flow rate was set to 1ml/h. For internal lumen content flow rate, we estimated that the lumen volume of a 2w old mouse colon is about 15ul. Flow rates of 1 to 60ul/h had no visible effect on colonic viability. We set up the lumen flow rate in our experiments to 30ul/h. The volume of the embryonic colon is much smaller, thus flow rate should be adjusted accordingly.

Lumen medium:

The luminal medium flow needs to enable bacterial growth, yet it should fit with the physiological requirements of the gut epithelial layer. Indeed, infusion of microbes

resuspended in their basal microbial growth medium to the gut cultures damaged the IEC integrity. Thus, microbial cultures were resuspended in the same tissue culture growth medium used for external flow, which we found to fit with microbial growth as well. To enable the growth of anaerobic microbes, the medium was incubated in the anaerobic chamber for 48h prior to the experiment. We titrated the microbial growth rate and found that these conditions allow growth of anaerobic microbes used in this study.

In a set of preliminary experiments, we aimed to mimic the physiologic consistency of the lumen content, while preserving proper flow through the gut. Supplementing the medium with thickening agents as pectin or cornstarch resulted in dehydration of the cultured tissue, and cause clogging of the output ports. Therefore these supplements were not included in the final experimentations setup.

Temperature in the chamber:

We set up the temperature in the gut culture device to 37°C. We used standard lab heat block, and placed an adapter copper plate on top. To improve heat transfer to the device, the copper plate was topped with a layer of heat-sink silicon compound (Chemplex 1381 DE, Lubritech). In our lab environment, setting the heat block to 43°C ensured a medium temperature of 37°C inside the device (temperature was measured by a digital thermometer and by a temperature-sensitive paper placed inside the chamber).

Bacterial cultures for ex-vivo colonization:

We evaluated the bacterial growth rate throughout the experiment. For the bacteria *C. ramosum*, loading the input syringe with microbial concentration of higher

than  $5 \times 10^7$  CFU/ml resulted in decrease in the bacterial medium pH within 2h, due to bacterial growth (pH=6.5, compare with pH=7.1 at the sterile medium control). Thus, for all microbes used in microbial colonization assays (2h culture), the microbial load was between 1 to  $3 \times 10^7$  CFU/ml.

#### Culture duration:

Most of the preliminary experiments performed using the air-liquid interface method involved culture of embryonic or neonatal small and large intestinal fragments for several days (usually 1 to 5 days). The external tissue structure was mostly maintained, as well as spontaneous peristalsis and most of the mucosa and sub-mucosal layers (evaluated by standard H&E histology and immune-staining of immunological markers). However, the fine structure of the intestinal epithelium was damaged in long-term cultures (we noticed that the small intestine villi were more sensitive to long-term culture than the colonic IEC). Using the gut culture device improved tissue structure and viability, and allowed culture of larger, and more developed, intestinal fragments. Conservatively, the experiments described in the main text lasted no longer than 24 hrs for colons (and mostly between 2 to 6h).

## SUPPLEMENTARY FIGURE LEGENDS

**Figure S1 (related to Fig. 1):** Scale drawings of the 3D printed parts used for replica molding are shown here. The mold for the lid is shown from the side in (A) and from the top in (C). The mold for the wells is shown from the side in (B) and from the top in (D). The frame for the two molds is shown in (E). The way in which the mold frame is attached to the mold prior to molding is shown in (F). The positions for insertion of input and output ports are indicated by white/black dots, respectively (F). All dimensions are in millimeters.

**Figure S2 (related to Fig. 1):** (A) Histological analysis of small intestinal tissue structure (hematoxylin and eosin (H&E), left) and mucus production (Periodic acid-Schiff (PAS), right), comparing freshly dissected tissues (up) or tissues cultured for 2h in the gut culture device (down). Data are representative of more than three independent experiments. Scale bar = 100 $\mu$ m. (B) Immunofluorescence staining for E-cadherin (green) and confocal imaging of small intestinal tissues cultured for 2h. Scale bar = 40 $\mu$ m.

**Figure S3 (related to Fig. 1):** (A) Immunofluorescence staining of Mucin-2 and Cytokeratin-18 (top), E-cadherin (middle) and Ki-67 (bottom), and confocal imaging of freshly dissected colon tissues, and tissues cultured for 2/12/24h in the gut culture device. Representative images of more than three independent experiments. Scale bar = 40 $\mu$ m. (B) Whole-mount staining and confocal imaging of Tuj1 (red) and nNOS (green)

showing the myenteric and submucosal plexus of the enteric nervous system in freshly dissected colons, or following 8/24h in the gut culture device. (C) Immunofluorescence staining of the enteroendocrine marker Chromogranin-A and confocal imaging of freshly dissected colon tissues, and tissues cultured for 2/12/24h in the gut culture device.

**Figure S4 (related to Fig. 4):** Analysis of colonic RORg<sup>+</sup> Treg frequencies from *Il6*-deficient mice or control littermates. P value was determined by unpaired Student's t test. Each point is an individual mouse. Data are representative of two independent experiments.

## **SUPPLEMENTARY MOVIE LEGENDS**

### **Movie S1 (related to Fig. 1): Operation of the gut organ culture system**

Movie S1 illustrates the use of the gut organ culture device. The following text is a caption for its successive frames.

#### **Part 1: Device fabrication**

1. One-time step: generate a mold master of the culture device and lid, using a 3D printer

\* The AutoCad design file and 3D printing instructions were deposit at [GitHub.com](https://github.com)

2. Prepare the mold: attach the frame to the base using binder clips

3. Mix together PDMS base and cross-linker in a 10:1 ratio and pour into the mold

4. Remove air bubbles: de-gassed in a vacuum chamber for 30 minutes

5. Bake: overnight incubation at 55°C until the PDMS is fully cured

6. Removed the solid PDMS slabs from the molds. Attach the PDMS slabs to a glass slide using all-purpose silicone sealant. Cure overnight at room temperature.

7. Prepare input/output ports: use blunt needles (1.5" long), 22G for lumen flow and 18G for external medium flow. Attach Luer lock to barbed tubing adaptor.

8. Connect input/output ports: for each channel, punch holes in appropriate locations using 18G and 21G needles (side by side, for both input and output; Fig.1A, Fig.S1).

Thread blunt needles through the holes, for a total of 24 input/output ports (6 lumen input + 6 lumen output + 6 external medium input + 6 external medium output).

9. Seal the area around each needle (surrounding the device) using silicone sealant and cure overnight.
10. Knott surgical threads around the luminal input and output ports. This will be used later to secure the gut segments in place.
11. Sterilized the entire system by dry-cycle autoclaving at 121°C for 20 minutes.
12. Fabricate the device lid: repeat the process for the device lid, using the lid mold. Connect the gas entry port to the lid (14G flat-end needle) and an additional 20G flat-end needle in the opposite side of the lid, for gas pressure release.

## **Part 2: Gut culture setup**

1. Prepare tubing: Cut Tygon PVC tubing to the appropriate length (from the input/output ports to the pumps). Attach Luer lock adaptor (female) to each tube (total of 24 tubes). Sterilized by dry-cycle autoclaving.
2. Culture medium input: In the hood, load syringes with sterile, tissue culture medium. Connect sterile Tygon tube to the syringes.
3. Luminal input: Resuspend the desired luminal stimulation in sterile tissue culture medium. In example, for microbial stimulation, spin down microbial cultures and resuspend in sterile tissue culture medium. For anaerobic microbes, de-gas culture medium in anaerobic chamber for 48h before use. Load input syringes with the luminal medium. Connect sterile Tygon tube to the syringes.
4. Load input pumps (infusion) with the pre-filled input syringes. Load output pumps (withdrawal) with empty syringes and tubing. Set the infusion/withdrawal flow rate.

5. Place the adaptor copper plate on top of a standard lab hot plate. Set temperature to 43°C (for a final 37°C in the device; adapt according to the lab room temperature). Apply a layer of heat-sink silicon compound for optimal heat transfer.
6. Connect a compressed gas cylinder containing medical grade mixture of 5% CO<sub>2</sub> and 95% O<sub>2</sub> to a standard oxygen humidifier, pre-filled with water. Connect one end of a sterile Tygon tube to the humidifier, and the other end to a 0.22µm syringe filter.
7. Prepare the gut culture device: in the hood, flush the input/output ports of the device with sterile tissue culture medium, to remove residual air and ensure a proper flow through the ports. Wash the device channels with sterile mediums. Fill channels with the culture medium (enough to cover the input/output ports).

### **Part 3: Connecting the gut fragment to the device**

1. Dissect the intestinal tissue. In example, for 14d old mice, dissect whole colon, or a 4cm long fragment of the small intestine.

In the hood, under a dissection microscope:

2. Gently flush the solid lumen content. Transfer to a plate containing clean medium.
3. Transfer the dissected gut fragments to the culture device. Plug the gut fragments into the luminal input/output ports. Maintain directionality of the intestinal fragments (i.e., connect the proximal end of the colon to the input port, and the distal end to the output port).

4. Fix the gut fragments over the luminal input and output ports using the pre-positioned surgical thread.

5. Cover the device using the sterile, pre-fabricated, lid.

#### **Part 4: Connect the device to the system setup**

1. Place the covered device on the adaptor plate.

2. Fix the device over the plate. Use a plastic cover lid and screws (see movie S1).

3. Purge the input tubing to remove the residual air.

4. Connect input and output tubing to the input/output ports (total of 24 tubes)

5. Start gas flow, and connect to the gas entry port using a sterile Tygon tube (from the gas filter to the device lid).

6. Start input flow of the external culture medium (1ml/h infusion and withdrawal). Make sure that the medium level does not completely cover the gut fragment.

7. Luminal medium flow: Gently purge the lumen with the luminal medium input. Start input flow of the luminal medium (30ul/h infusion and withdrawal).

#### **Movie S2 (related to Fig. 1): The enteric nervous system is maintained in the gut organ culture system**

MovieS2 is a 3D reconstruction of the enteric nervous system in freshly dissected colon tissues and in colon cultured for 8/24h. Whole mount staining of Tuj1 and nNOS followed by confocal microscopy. Z-stack images were acquired on an Olympus Fluoview Confocal microscope (1um intervals), and 3D images were reconstructed using Imaris.

**Movies S3-4 (related to Fig. 1): Spontaneous peristalsis contractions in the gut organ culture system**

Movies S3-4 illustrates the peristalsis contractions of cultured colons (MovieS3) and small-intestines (MovieS4) in the gut culture device.

**Movie S5 (related to Fig. 1): Time lapse imaging using the gut organ culture system**

MoviesS5 illustrates a proof-of-principle of using the gut culture system in time-lapse imaging. Colons were dissected from CX3CR1-GFP and CD4-RFP mice, and connected to the gut organ culture device (see 'Methods'). Tissues were scanned at 3um Z-stack intervals every 40 seconds, on an Olympus Fluoview Confocal microscope. This 40 minutes movie was acquired after 5 hours organ culture period. Z-stacks and time-lapse movies were generated using Imaris.

## KEY RESOURCES TABLE

REAGENT or RESOURCE	SOURCE	IDENTIFIER
<b>Antibodies</b>		
Anti-mouse CD45 Brilliant Violet 605	Biolegend	Cat#103140
Anti-mouse CD19 APC Cy7	Biolegend	Cat#115530
Anti-mouse TCR $\beta$ chain Pacific blue	Biolegend	Cat#109226
Anti-mouse TCR $\gamma\delta$ APC	Biolegend	Cat#118116
Anti-mouse/human CD11b Percp Cy5.5	Biolegend	Cat#101228
Anti-mouse CD11c PE Cy7	Biolegend	Cat#117318
Anti-mouse Ly6c FITC	Biolegend	Cat#128006
Anti-mouse CD103 PE	Biolegend	Cat#121406
Anti-mouse F4/80 Alexa 700	Biolegend	Cat#123130
Anti-mouse CD4 Percp Cy5.5	Biolegend	Cat#100434
Anti-mouse TCR $\beta$ chain PE Cy7	Biolegend	Cat#109222
Anti-mouse Helios Pacific blue	Biolegend	Cat#137220
Anti-mouse/rat Foxp3 APC	Affymetrix/eBioscience	Cat#17-5773-82
Anti-mouse/human ROR gamma (t) PE	Affymetrix/eBioscience	Cat#12-6988-80
Anti-mouse Mucin2	Santa-Cruz Biotechnology	Cat#sc-15334
Anti-mouse Cytokeratin 18	Santa-Cruz Biotechnology	Cat#sc-51582
Anti-mouse Ki-67	BD Bioscience	Cat#556003
Anti-mouse E-cadherin (CD324)	Biolegend	Cat#147302
Anti-mouse CX3CR1	Biolegend	Cat#824001
Anti-mouse Chromogranin-A	AbCam	Cat#ab15160
Anti-mouse nNOS	AbCam	Cat#1376
Anti-mouse Tuj1 (Tubulin beta-3)	Biolegend	Cat#802001
donkey anti-goat Cy5	Jackson ImmunoResearch labs	Cat#705-175-147
donkey anti-rabbit Cy3	Jackson ImmunoResearch labs	Cat#711-165-152
donkey anti-mouse Cy5	Jackson ImmunoResearch labs	Cat#715-175-150
donkey anti-rat Cy5	Jackson ImmunoResearch labs	Cat#712-175-150
<b>Chemicals, Peptides, and Recombinant Proteins</b>		
Collagenase, Type II	Thermo Fisher Scientific	Cat#17101015
Dispase	Thermo Fisher Scientific	Cat#17105-041
Bacto Yeast Extract	BD, Becton, Dickinson and Company	Cat#212750
Bacto Proteose Peptone No.3	BD, Becton, Dickinson and Company	Cat#211693

Brucella 5% SB HEMIN VIT K1 plates	BBL, Becton, Dickinson and Company	Cat#6217793
TSA II 5% SB	BBL, Becton, Dickinson and Company	Cat#6189554
FoxP3/Transcription Factor Staining Buffer Set	Affymetrix/eBioscience	Cat#00-5523-00
<b>Critical Commercial Assays</b>		
<b>Deposited Data</b>		
Raw and normalized data	This paper	GEO: GSE92471
<b>Experimental Models: Cell Lines</b>		
<b>Experimental Models: Organisms/Strains</b>		
SPF mice	The Jackson Laboratory	C57BL/6
SPF mice	The Jackson Laboratory	NOD (Non-obese diabetic)
Mouse, Germ-free, C57BL/6	GF C57BL/6 origin from L. Bry, colony housed in isolators at the HMS GF animal facility	GF C57BL/6
Mouse, Germ-free, SW	GF Swiss Webster colony housed in isolators at the HMS GF animal facility	GF Swiss Webster
Mouse, SW, SFB mono-colonized	SFB mono-colonized Swiss Webster colony housed in isolators at the Kasper lab GF animal facility	SFB mono-colonized
Bacterial strains	This paper	Table S3
<b>Recombinant DNA</b>		
<b>Sequence-Based Reagents</b>		
Cy-5 or Alexa-568 conjugated EUB338 probe for Fluorescence In-Situ Hybridization (FISH): 5'-GCTGCCTCCCGTAGGAGT-3'	This paper	EUB388
Alexa-488 conjugated SFB-specific FISH probe: 5'-GGTACTTATTGCGTTTGCGACGGCAC-3'	This paper	SFB probe
<b>Software and Algorithms</b>		

Multiplot	Scott P. Davis (Tempero Pharmaceuticals), in collaboration with Christophe Benoist (Harvard Medical School)	<a href="http://gparc.org/view/urn:lsid:127.0.0.1:gene-patternmodules:4:1.5.20">http://gparc.org/view/urn:lsid:127.0.0.1:gene-patternmodules:4:1.5.20</a>
Gene-E	The Broad Institute	<a href="https://software.broadinstitute.org/GENE-E/">https://software.broadinstitute.org/GENE-E/</a>
Enrichr	Chen, E.Y., et al., (2013). BMC. Bioinformatics. 14, 128	<a href="http://amp.pharm.mssm.edu/Enrichr/">http://amp.pharm.mssm.edu/Enrichr/</a>
Imaris	Bitplane	Imaris version 8.3
Fiji (ImageJ)	NIH	ImageJ version 2
GraphPad Prism	GraphPad Software	<a href="https://www.graphpad.com/scientific-software/prism/">https://www.graphpad.com/scientific-software/prism/</a>
<b>Other</b>		

Figure 1

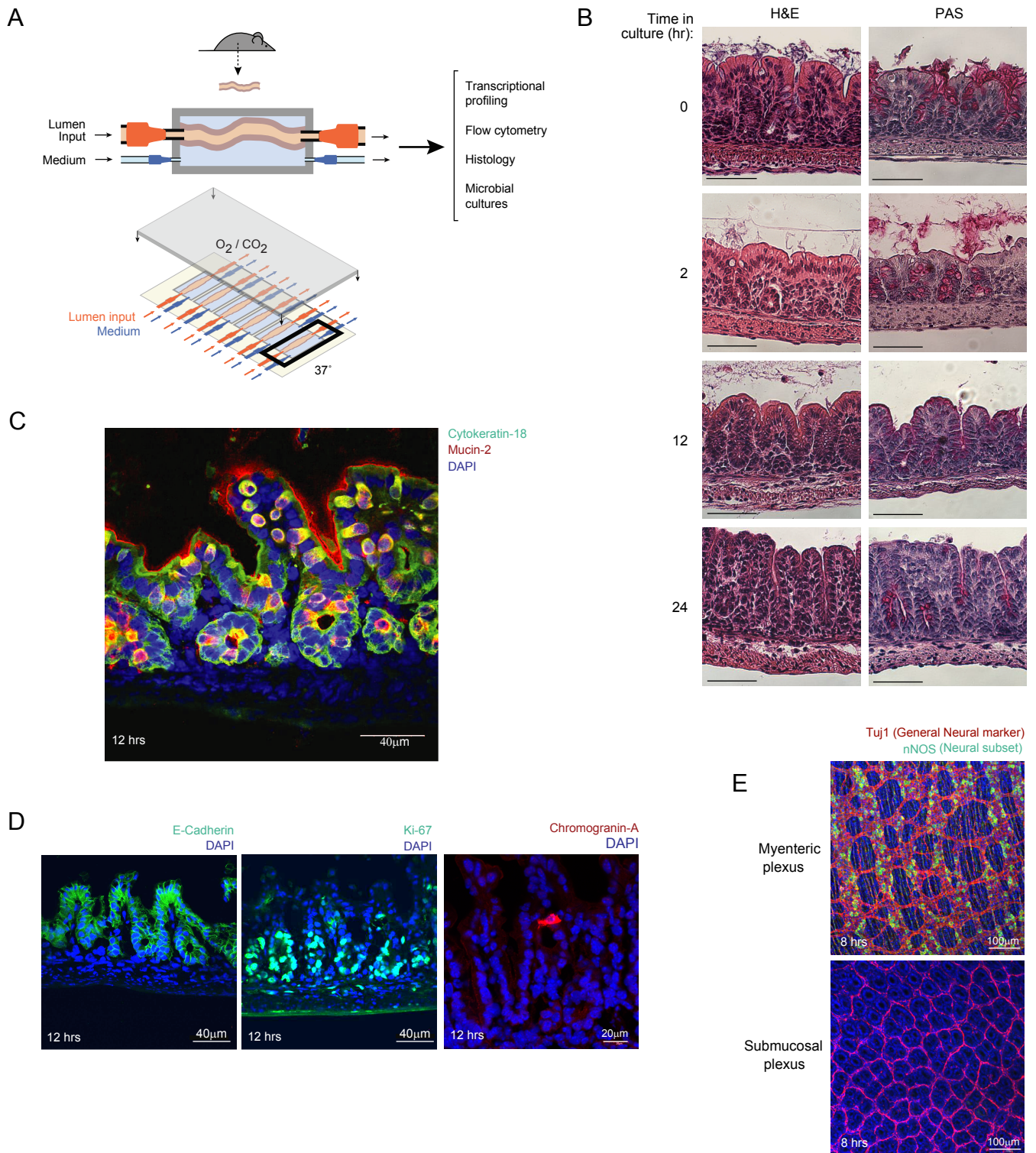


Figure 2

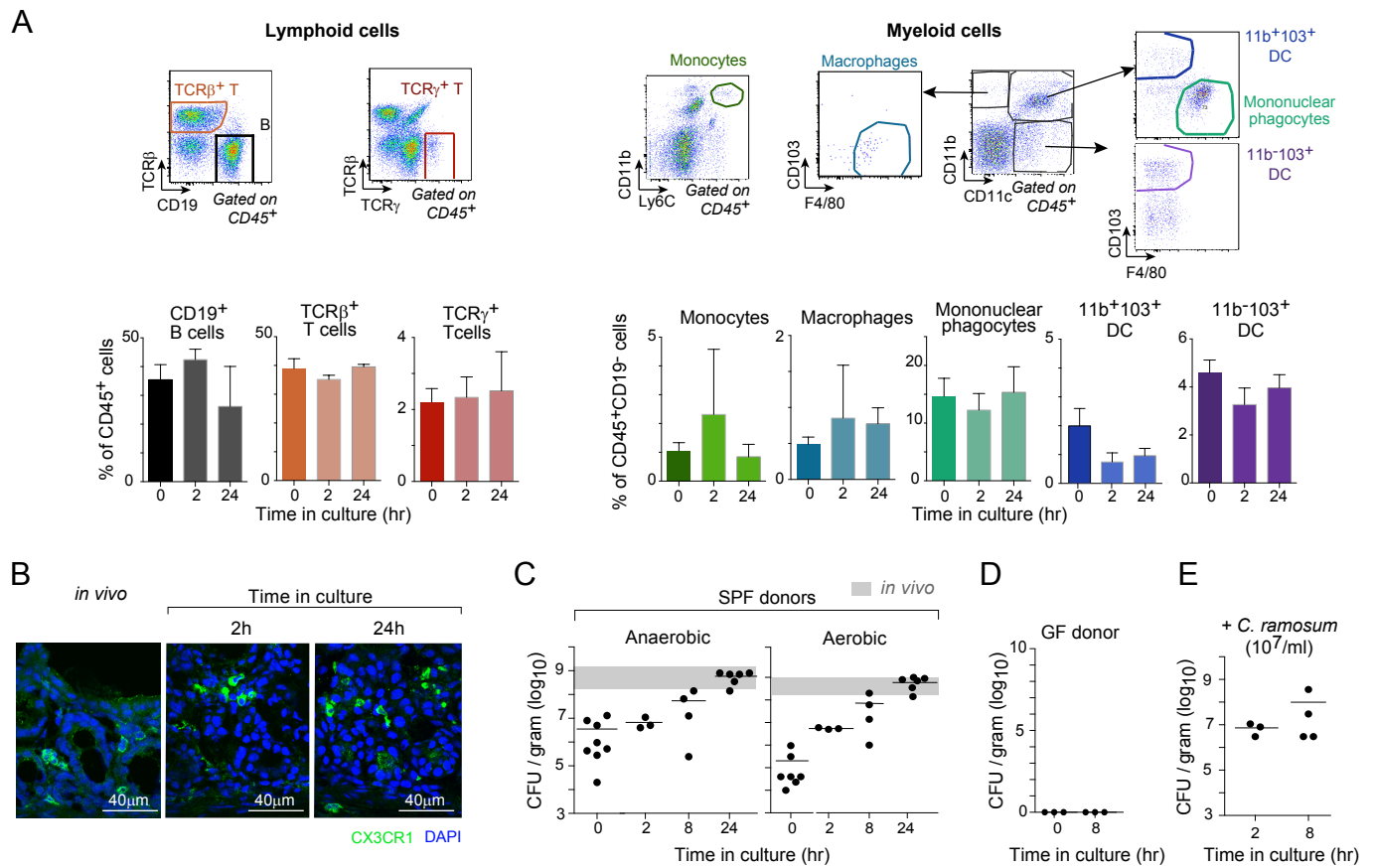
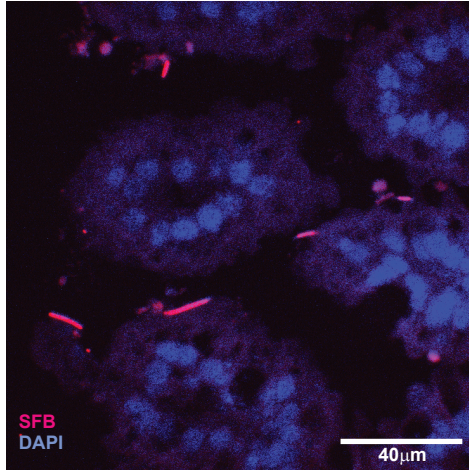
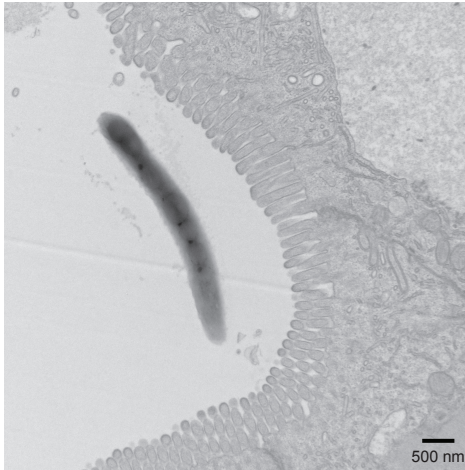


Figure 3

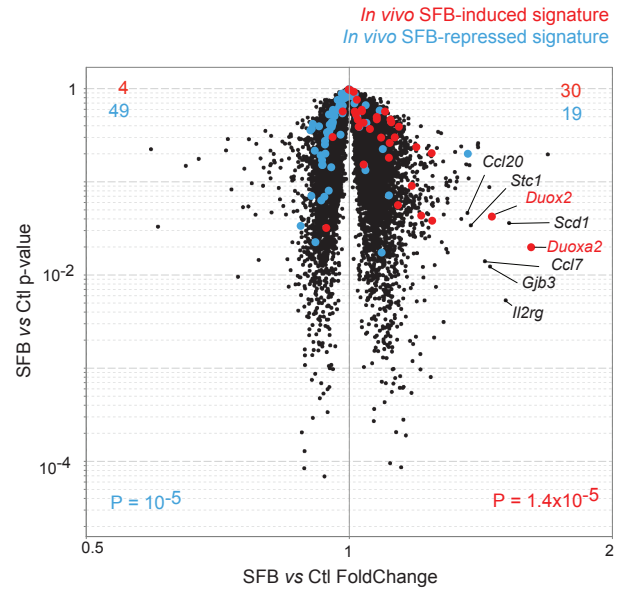
A



B



C



D

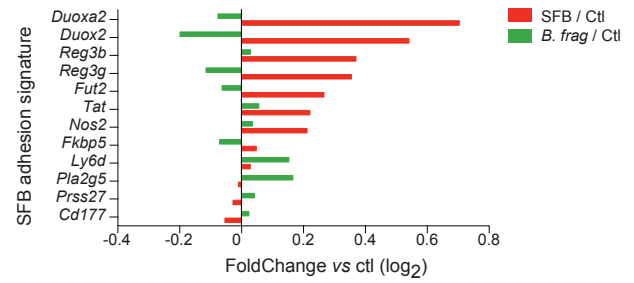


Figure 4

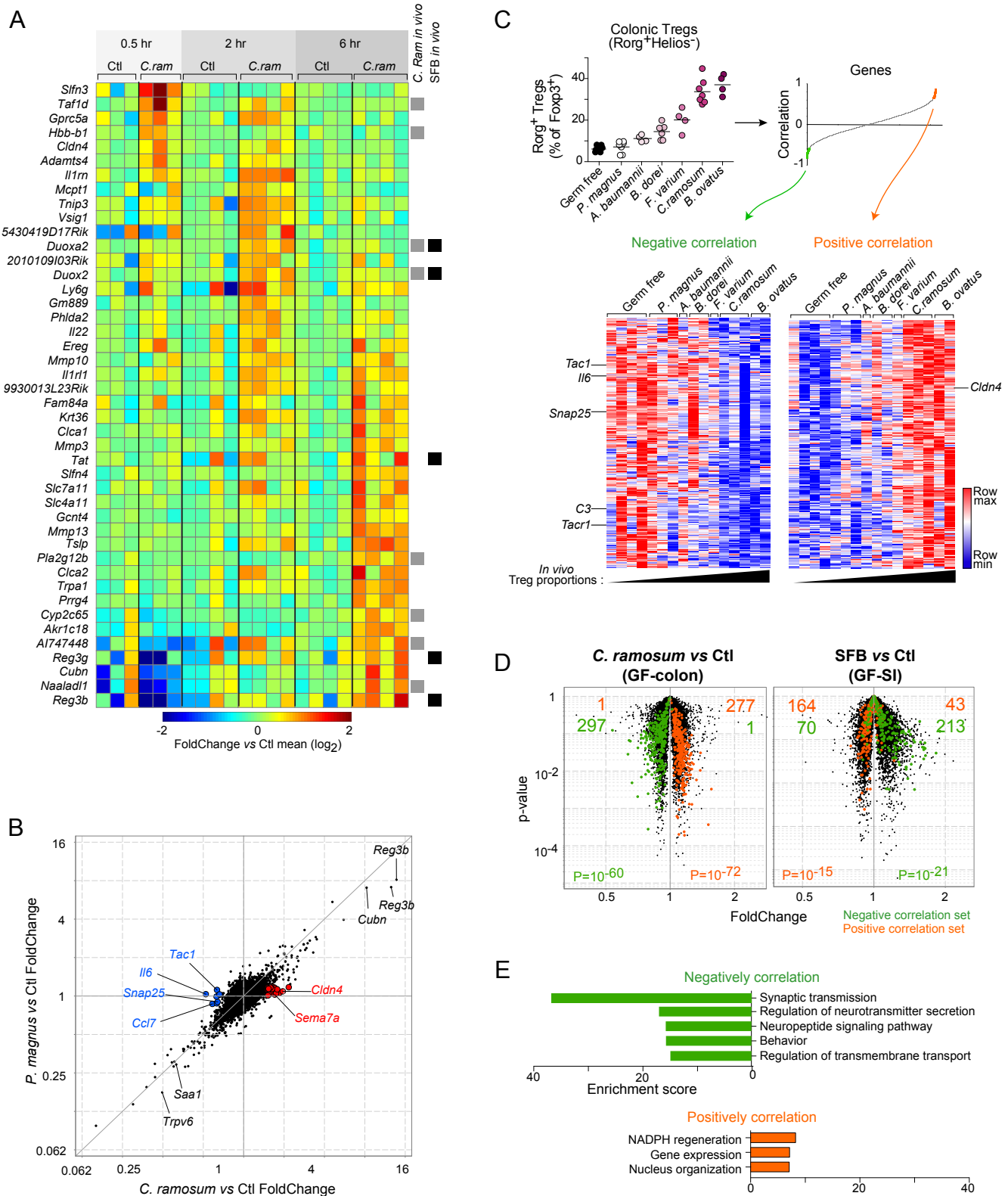


Figure 5

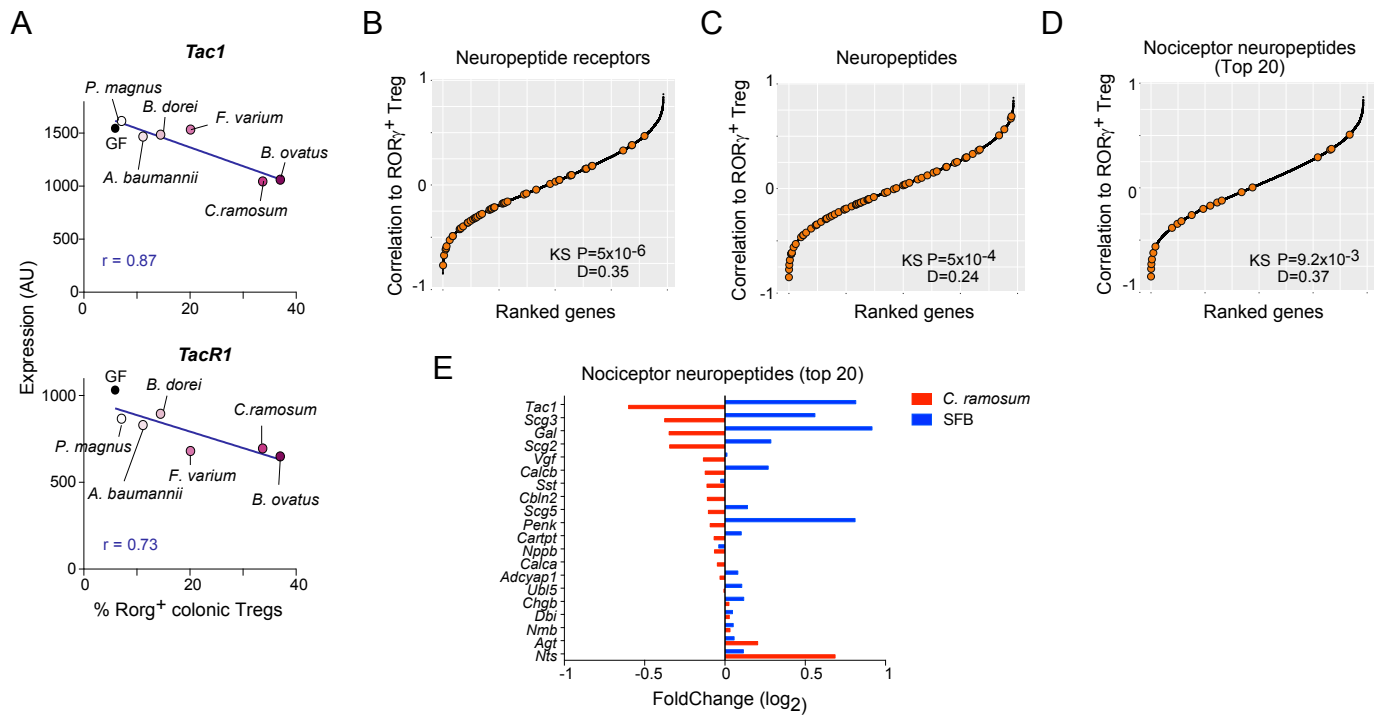


Figure 6

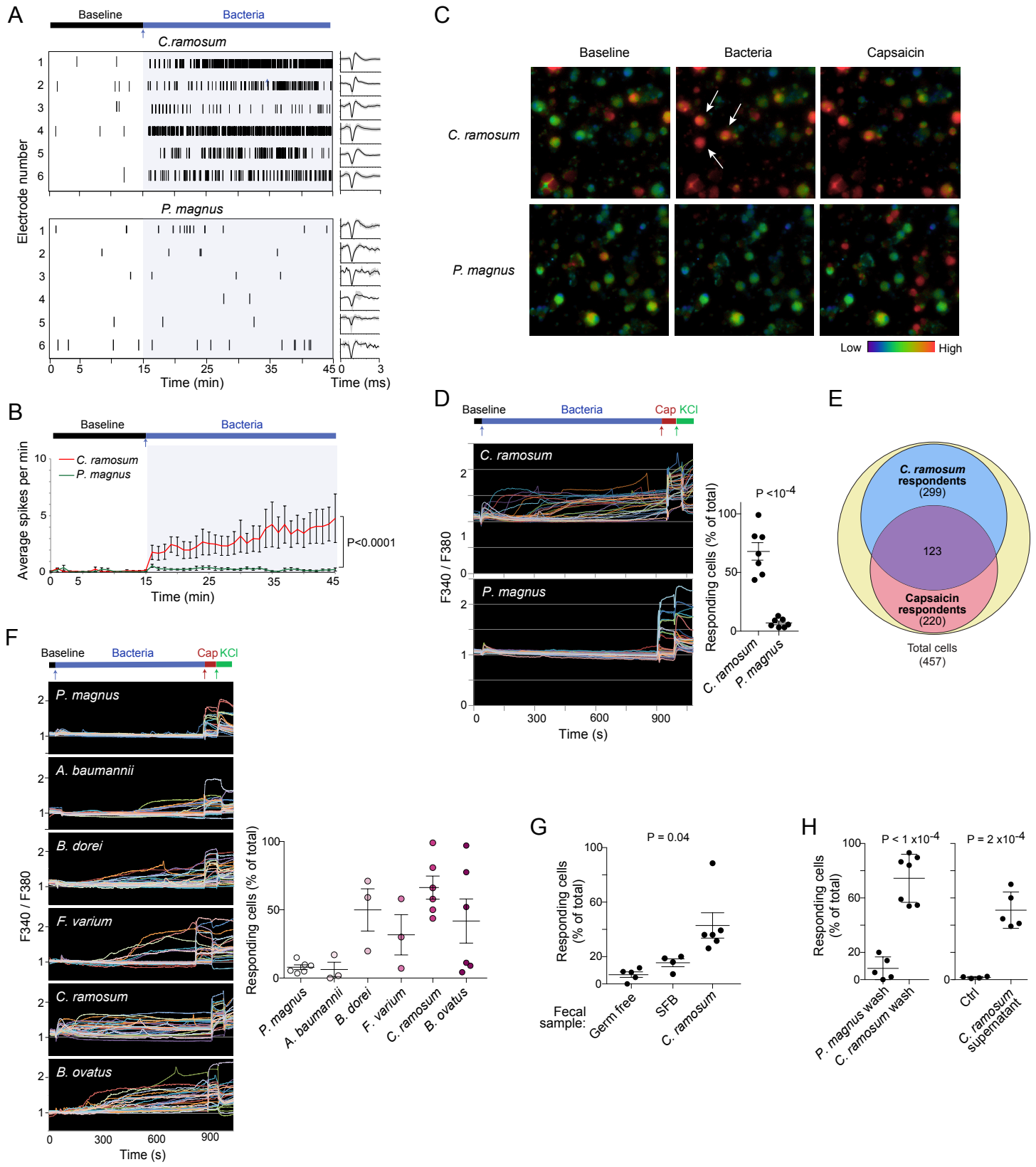


Figure 7

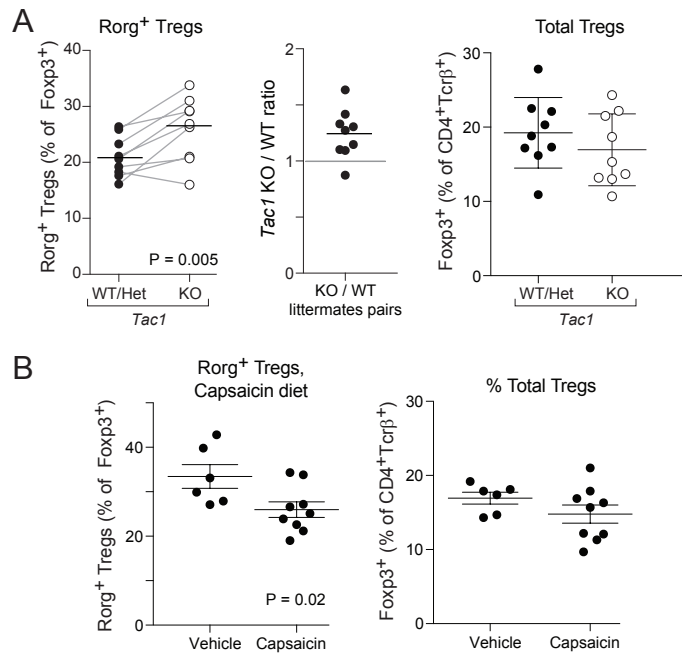


Figure S1  
Related to figure1

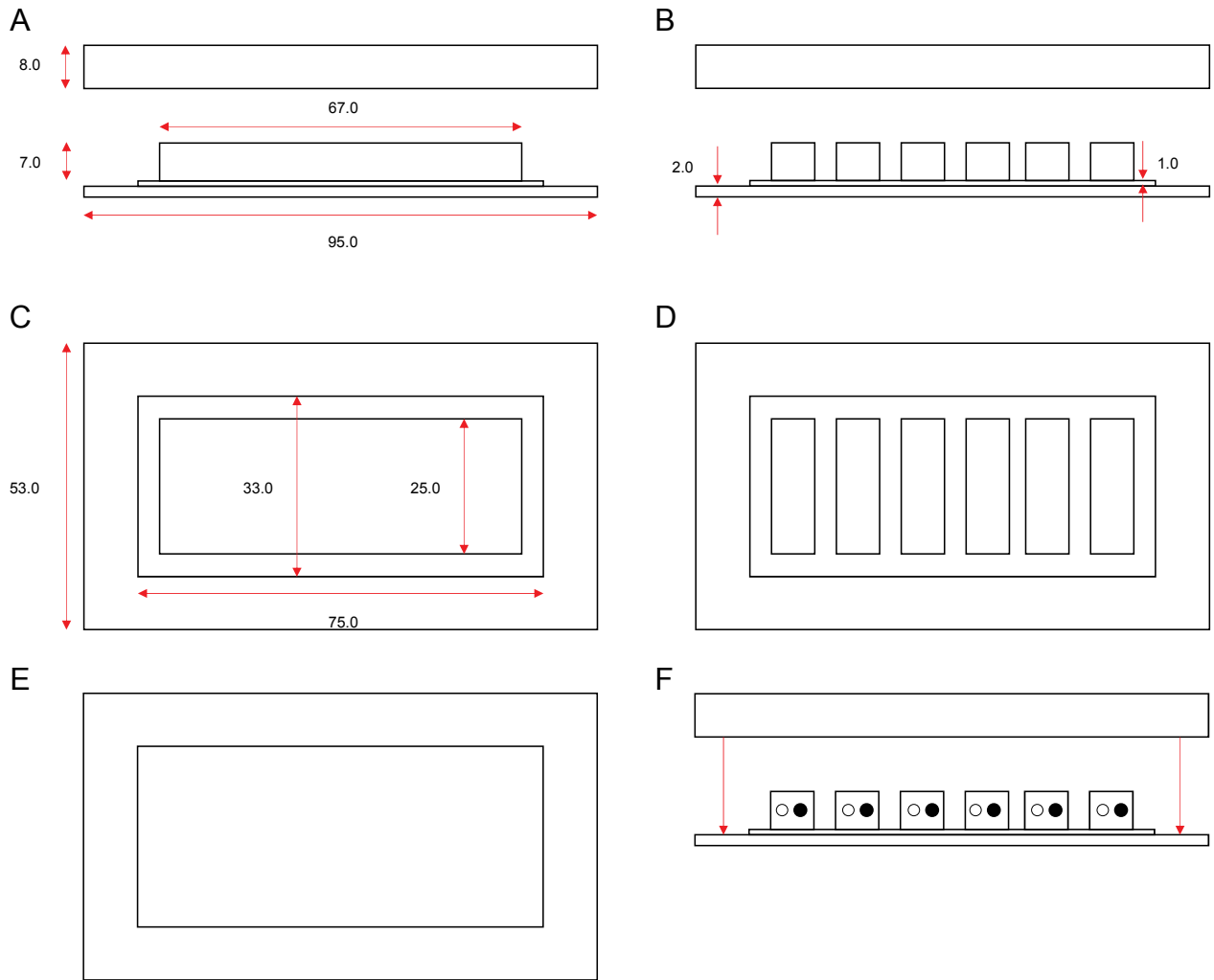
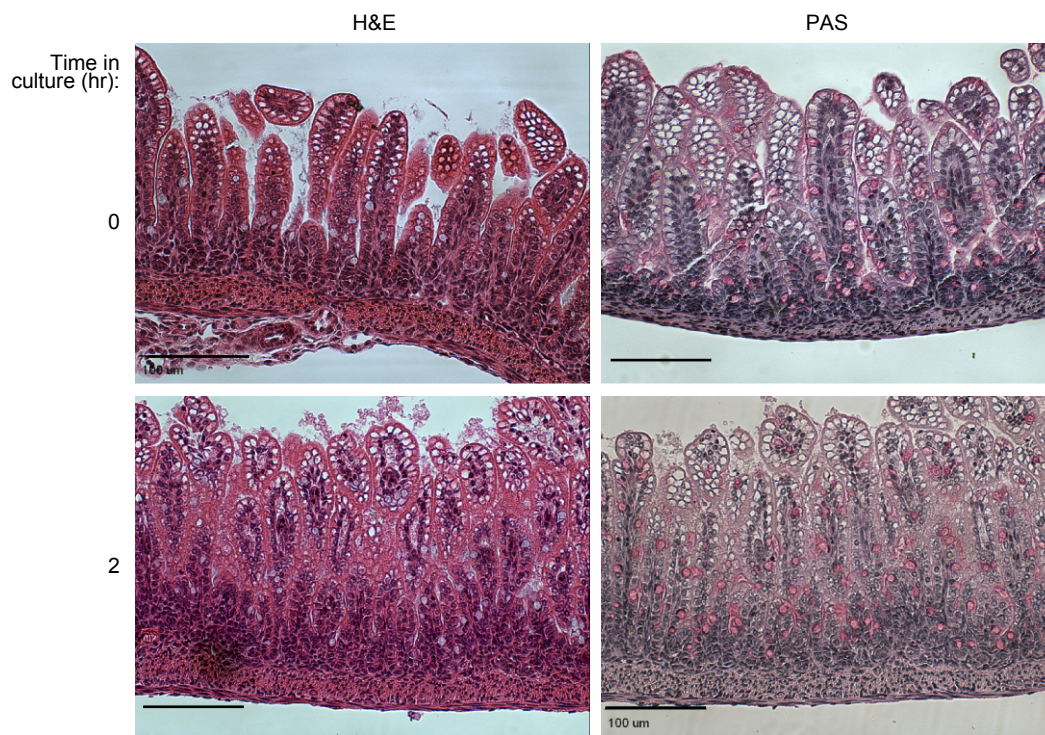


Figure S2  
Related to figure1

A



B

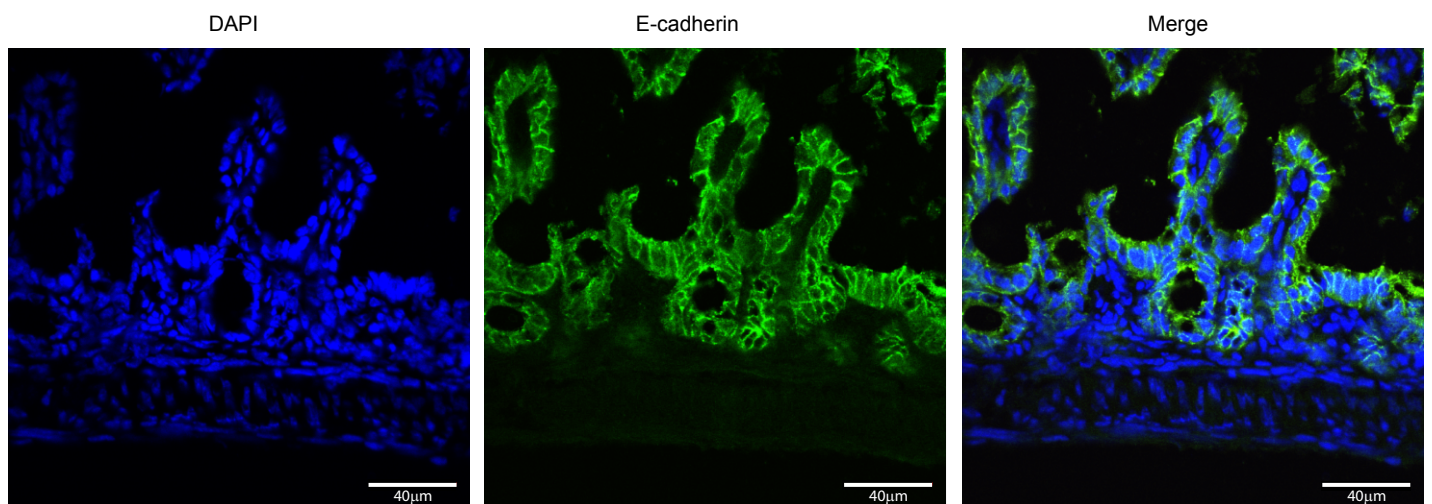


Figure S3  
Related to figure1

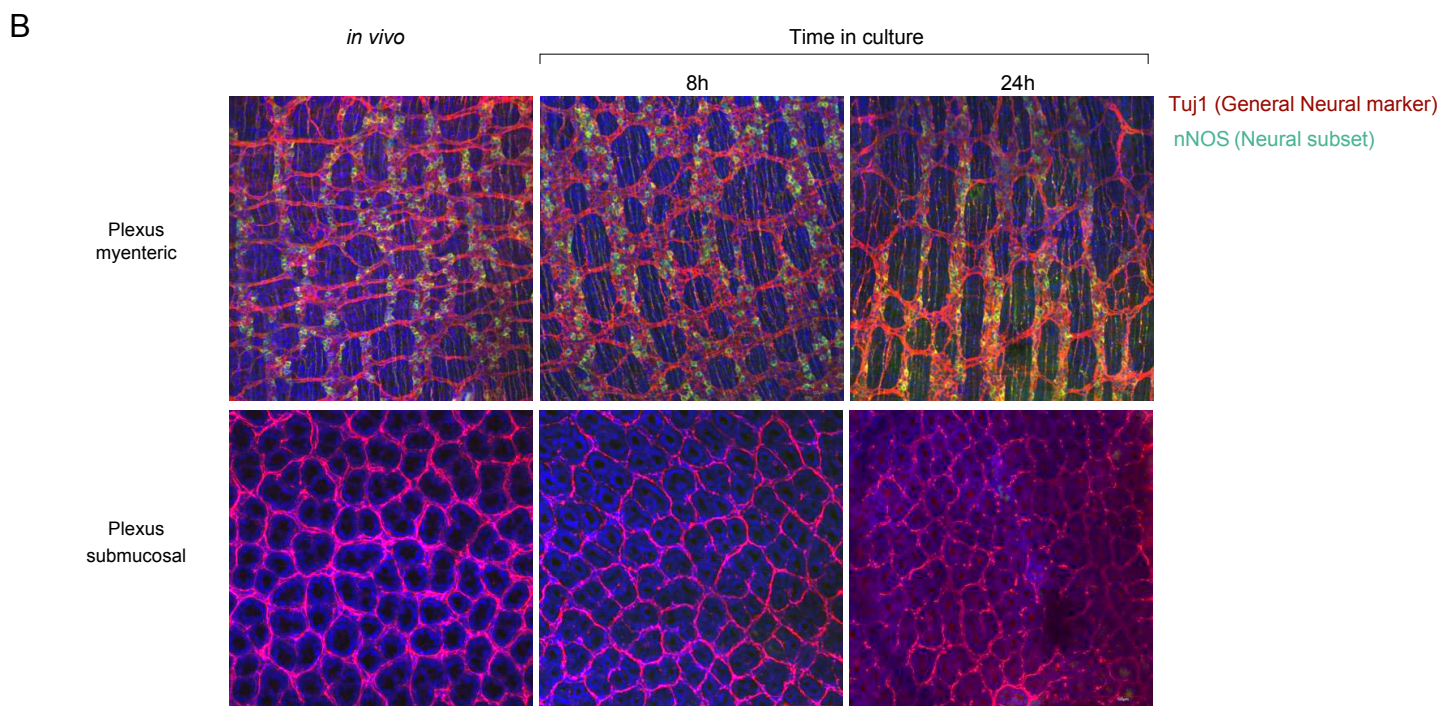
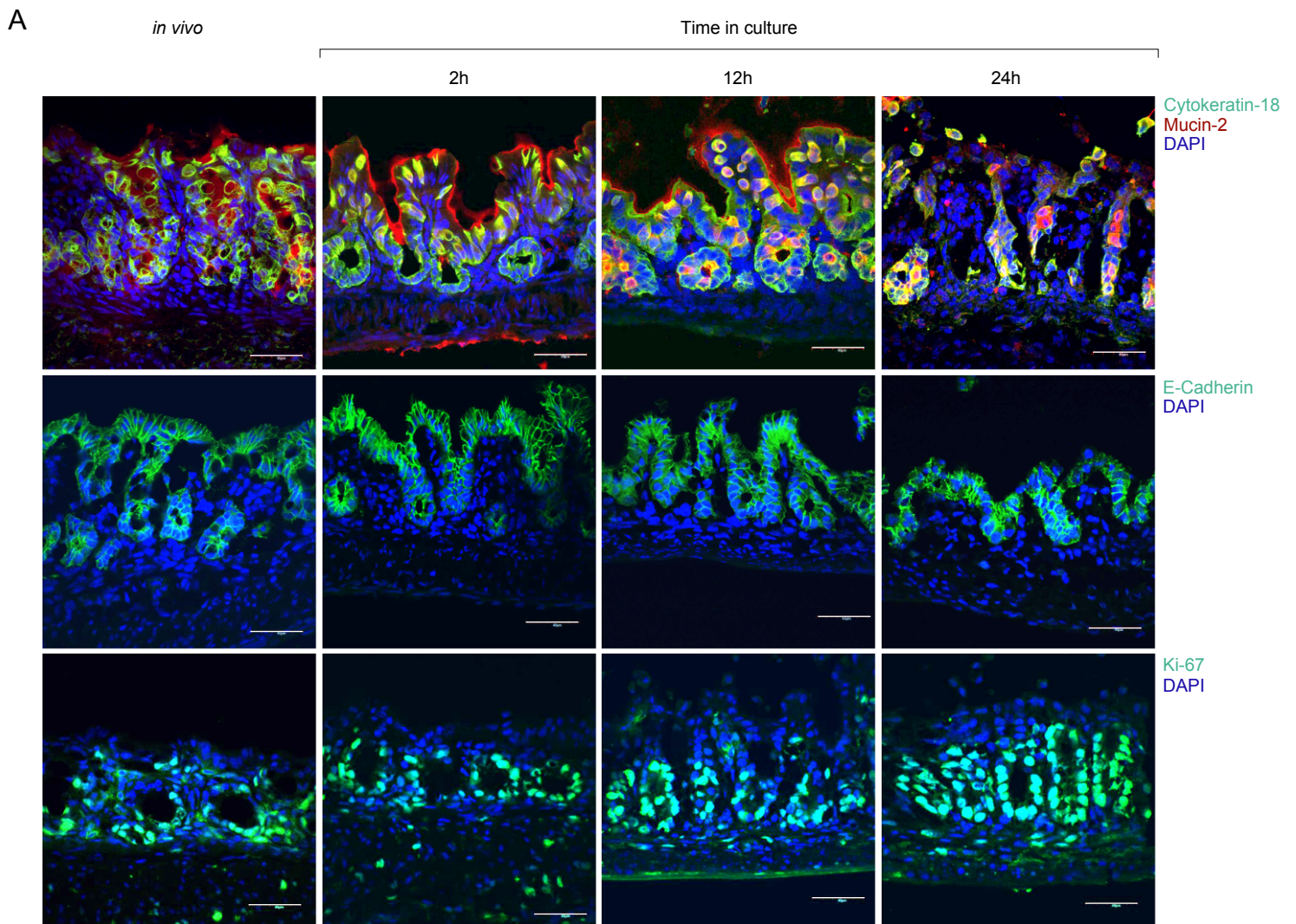
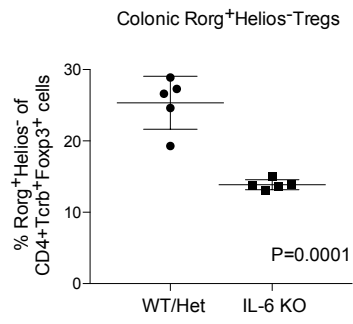
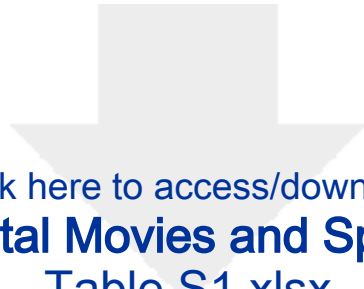




Figure S4  
Related to figure 4





[Click here to access/download](#)

**Supplemental Movies and Spreadsheets**  
**Table S1.xlsx**





[Click here to access/download](#)

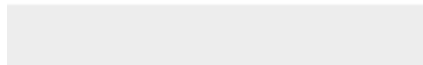
**Supplemental Movies and Spreadsheets**  
**Table S2.xlsx**





Click here to access/download

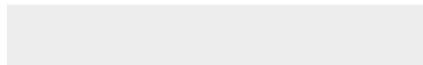
**Supplemental Movies and Spreadsheets**  
Table\_S3.xlsx





[Click here to access/download](#)

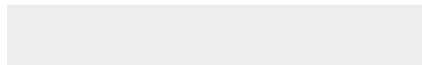
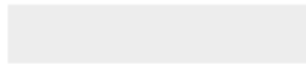
**Supplemental Movies and Spreadsheets**  
**MovieS1.mp4**





[Click here to access/download](#)

**Supplemental Movies and Spreadsheets**  
**MovieS2.mp4**





[Click here to access/download](#)

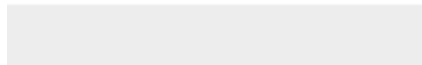
**Supplemental Movies and Spreadsheets**  
**MovieS3.mp4**





[Click here to access/download](#)

**Supplemental Movies and Spreadsheets**  
**MovieS4.mp4**





[Click here to access/download](#)

**Supplemental Movies and Spreadsheets**  
**MovieS5.mp4**

